Numerical Study of Coupled Water and Vapor Flow, Heat Transfer, and Solute Transport in Variably-Saturated Deformable Soil During Freeze-Thaw Cycles

Huang, Xiang
Rudolph, David L.

To be published in: Water Resources Research

DOI to publisher's version: 10.1029/2022WR032146

Water Resources Research

RESEARCH ARTICLE
10.1029/2022WR032146

Numerical Study of Coupled Water and Vapor Flow, Heat Transfer, and Solute Transport in Variably-Saturated Deformable Soil During Freeze-Thaw Cycles

Xiang Huang[1,2] **and David L. Rudolph**[2]

[1]Earth and Environmental Sciences Division, Los Alamos National Laboratory, Los Alamos, NM, USA, [2]Department of Earth and Environmental Sciences, University of Waterloo, Waterloo, ON, Canada

Key Points:

- Coupled modeling of thermal-hydraulic-mechanical-chemical processes improves our understanding of the hydrological dynamics in the cryo-subsurface
- A bidirectional exchange between saturated groundwater and unsaturated soil water can be a significant process during freeze-thaw cycles
- Freeze-thaw can generate highly variable deformation and solute transport behavior in fine-grained frost susceptible sediments like silt

Supporting Information:

Supporting Information may be found in the online version of this article.

Correspondence to:

X. Huang,
xiang.huang@uwaterloo.ca

Citation:

Huang, X., & Rudolph, D. L. (2023). Numerical study of coupled water and vapor flow, heat transfer, and solute transport in variably-saturated deformable soil during freeze-thaw cycles. *Water Resources Research*, *59*, e2022WR032146. https://doi.org/10.1029/2022WR032146

Received 6 FEB 2022
Accepted 20 JUL 2023

Abstract As climate change intensifies, soil water flow, heat transfer, and solute transport in the active, unfrozen zones within permafrost and seasonally frozen ground exhibit progressively more complex interactions that are difficult to elucidate with measurements alone. For example, frozen conditions impede water flow and solute transport in soil, while heat and mass transfer are significantly affected by high thermal inertia generated from water-ice phase change during the freeze-thaw cycle. To assist in understanding these subsurface processes, the current study presents a coupled two-dimensional model, which examines heat conduction-convection with water-ice phase change, soil water (liquid water and vapor) and groundwater flow, advective-dispersive solute transport with sorption, and soil deformation (frost heave and thaw settlement) in variably saturated soils subjected to freeze-thaw actions. This coupled multiphysics problem is numerically solved using the finite element method. The model's performance is first verified by comparison to a well-documented freezing test on unsaturated soil in a laboratory environment obtained from the literature. Then based on the proposed model, we quantify the impacts of freeze-thaw cycles on the distribution of temperature, water content, displacement history, and solute concentration in three distinct soil types, including sand, silt and clay textures. The influence of fluctuations in the air temperature, groundwater level, hydraulic conductivity, and solute transport parameters was also comparatively studied. The results show that (a) there is a significant bidirectional exchange between groundwater in the saturated zone and soil water in the vadose zone during freeze-thaw periods, and its magnitude increases with the combined influence of higher hydraulic conductivity and higher capillarity; (b) the rapid dewatering ahead of the freezing front causes local volume shrinkage within the non-frozen region when the freezing front propagates downward during the freezing stage and this volume shrinkage reduces the impact of frost heave due to ice formation. This gradually recovers when the thawed water replenishes the water loss zone during the thawing stage; and (c) the profiles of soil moisture, temperature, displacement, and solute concentration during freeze-thaw cycles are sensitive to the changes in amplitude and freeze-thaw period of the sinusoidal varying air temperature near the ground surface, hydraulic conductivity of soil texture, and the initial groundwater levels. Our modeling framework and simulation results highlight the need to account for coupled thermal-hydraulic-mechanical-chemical behaviors to better understand soil water and groundwater dynamics during freeze-thaw cycles and further help explain the observed changes in water cycles and landscape evolution in cold regions.

1. Introduction

A changing climate increases the variability in hydrologic dynamics within periglacial landforms and particularly in the subsurface, where freezing and thawing conditions can exist. For example, water (moisture) movement in freezing soils plays a crucial role in frost heave and subsequently thaw settlement, processes that must be considered while assessing slope stability in the construction of infrastructure such as paved roadways and buried pipelines and landform evolution (e.g., Huang et al., 2022; Williams & Smith, 1989). Subsurface water flow and storage dynamics in seasonally frozen soils are very different from those within the perennially frozen ground (permafrost) or in warmer regions with negligible frozen soil (e.g., Ireson et al., 2013; Zheng et al., 2002). Subsurface hydraulic and thermal properties, mass fluxes and stress-strain fields are usually affected by the cyclic formation of ice due to water-ice phase change during the annual freeze-thaw cycle. In addition, warming climate conditions result in changing hydrological processes, such as precipitation, evapotranspiration, and in particular, freeze-thaw cycles, which may also influence the thawing rate of permafrost and the depth of the frost zone (e.g., Evans et al., 2018; Kurylyk et al., 2014). However, what is not well understood are the feedbacks between these

hydrological drivers and freeze-thaw cycles, which control subsurface water flow and storage in seasonally frozen regions (e.g., Chen et al., 2019; Xie et al., 2021).

Soil freezing is a complicated phenomenon that involves the migration of liquid water toward the advancing freezing front, concomitant with the expansion of solid ice (e.g., excess ice, ice lenses/wedges) within the pore space, often leading to ground surface frost heave. Upon thawing, these processes reverse, as solid ice transforms into liquid water, resulting in water drainage and thaw settlement. The phase transition between ice formation and melting during the freeze-thaw cycles entails a large amount of fusion latent heat that provides high thermal inertia with significant implications on heat transfer, moisture mobility, and their availability in soils. In addition, freeze-thaw processes have been shown to be influenced by soil solute dynamics within the unfrozen water (e.g., Hayashi, 2013; Ireson et al., 2013). Investigation of the propagation of a freezing front, redistribution of water content, and associated features of interest in soil subjected to freeze-thaw cycles is often conducted through laboratory and/or field experiments. However, monitoring and characterization of all relevant variables and feedback mechanisms are challenging due to limitations of the monitoring equipment and the experimental execution in cold harsh environments (e.g., Williams & Smith, 1989; Zheng et al., 2002). In concert with experimental observations, models can be valuable auxiliary tools to close information gaps in observations in space and time and have become vital to exploring seasonal freeze-thaw processes in the soil ecosystem. This is true whether the research objective is related to mechanism verification based on observational data or predictive understanding utilizing synthetic analysis.

A progression of models has been developed in the past few decades to simulate freezing and thawing in the subsurface. However, these models tackle the freeze-thaw processes with different levels of complexity and generally can be categorized into three groups: thermal-hydrologic (TH) models, thermal-mechanical (TM) models, and thermal-hydro-mechanical (THM) models. Each of these approaches has its strengths and limitations on applicability to modeling frozen soil and permafrost studies. TH models can simulate multiphase, non-isothermal mass and energy transport in variably-saturated, non-deformable soils. Examples of these types of models include SHAW (e.g., Cui et al., 2020; Xie et al., 2021), Hydrus (Šimůnek et al., 2018), Sutra-ice (Evans et al., 2018; Kurylyk et al., 2014; McKenzie et al., 2007) and PFLOTRAN-ice (Karra et al., 2014), Smoker (Molson & Frind, 2015), among others (e.g., Grenier et al., 2018; Huang et al., 2016; Kelleners, 2020). This group does not consider mechanical deformation during the freeze-thaw period or solute transport processes. TM models present detailed thermal-mechanical dynamics in permafrost and building materials subjected to freeze-thaw action based on energy and momentum conservation, however, water migration and/or cryogenic suction are usually ignored (e.g., Loli et al., 2020; Žák et al., 2013). Models introduced by Arzanfudi and Al-Khoury (2018), and Thomas et al. (2009), for instance, are among the THM category and are generally formulated based on the theory of thermo-poroelasticity presented by Coussy (2005) and Selvadurai and Suvorov (2017). Most THM models are designed to predict the dynamics of soil water, temperature, and stress-strain in *saturated* frozen soils, and some also include solute transport processes (e.g., Zheng et al., 2002). Only a few of these THM models are suitable for describing freeze-thaw processes in unsaturated deformable soils (e.g., Huang & Rudolph, 2021) and their associated solute transport reactions (e.g., Frampton & Destouni, 2015; Mohammed et al., 2021). In order to more completely investigate and understand soil freeze-thaw behavior, there is a need to develop a coupled, multiphysics model encompassing the highly nonlinear processes involving the thermal, hydrological, mechanical, and chemical responses during freeze-thaw cycles.

It has been observed in many field/laboratory experiments that soil water (moisture) movement in freezing soils can lead to groundwater table decline (e.g., Cui et al., 2020; Zheng et al., 2002). Yet, the groundwater dynamics and their relations to the redistribution of soil water during the freeze-thaw period are largely unknown and not wholly accounted for in most numerical models (e.g., Chen et al., 2019; Cui et al., 2020). In many previous experimental and numerical studies, a fixed groundwater table is commonly imposed or assumed to study the pore water movement from the saturated zone through the unsaturated zone to the freezing front (e.g., Chen et al., 2019; Huang & Rudolph, 2021, 2022; Shoop & Bigl, 1997; Zheng et al., 2002). However, a fixed groundwater table boundary condition is an over-simplified representation of the groundwater recharge/discharge regime. This is particularly true during the annual frozen period when groundwater storage depletion can be the most active. In addition, a water flux boundary (e.g., free gravitational drainage or seepage boundary) is frequently applied to the bottom of unsaturated soil layers to simulate downward groundwater recharge (e.g., Kurylyk et al., 2014). This assumption does not permit the potential upward migration of pore water (cryosuction) and water vapor from the water table during freeze-thaw periods.

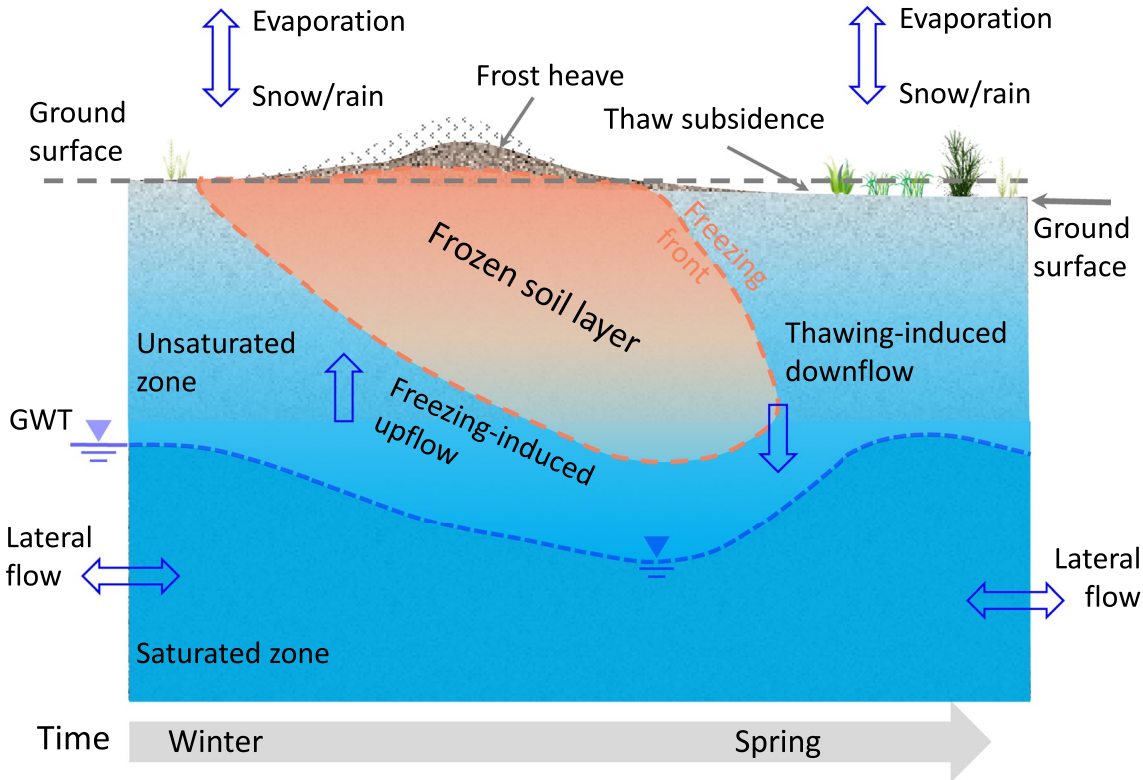

Figure 1. Schematic diagram of hydrological processes and groundwater regime within a soil profile during the late winter (freezing) and early spring (thawing) periods.

This paper proposes a fully coupled thermo-hydro-mechanical-chemical (THM-C) model for describing the coupling effect of water-vapor-heat movement and solute transport in variably-saturated, deformable soil subjected to freeze-thaw cycles, which have not been simultaneously considered in our previous studies (Huang et al., 2022; Huang & Rudolph, 2021, 2022). The model considers several crucial but commonly ignored physical processes such as cryosuction-induced water flow, vapor migration and evaporation-condensation, soil deformation, solute transport/adsorption, and freezing point depression. The numerical solution of these combined processes is conducted through the use of the COMSOL Multiphysics package (Comsol, 2017). The performance of the model structure is first verified by comparison with laboratory experimental observations from published literature. The two-dimensional model system is then used to quantify how the freeze-thaw cycles affect the evolution of temperature, water content, displacement history, and solute concentration in different soil textures. The factors influencing interactions between groundwater and soil water in the vadose zone are investigated and can provide a theoretical reference for practical engineering applications.

2. Methodology

2.1. Conceptual Formulation

The movement of soil moisture and groundwater in a deformable soil profile and its main hydrological processes during one seasonal freeze-thaw cycle is schematically illustrated in Figure 1. In addition to lateral groundwater outflow, the processes leading to groundwater level decline during the freezing stage include upward flow induced by freezing (cryosuction) and evaporation. In contrast, the processes leading to groundwater level rise are lateral groundwater inflow and downward flow contributed by thawing and precipitation during the thawing stage. A frozen zone enveloped by the freezing front is formed if the soil temperature is locally below the freezing point of the local soil water. In the frozen zone, the pore space is filled with a small amount of unfrozen liquid water, a large portion of solid ice, and a variable amount of soil gas. The accumulated ice content can continuously increase due to cryosuction and may expand the intrinsic pore space resulting in frost heave. The frozen zone gradually recedes when transitioning into the thawing stage, and the thawed-water will infiltrate downward

as groundwater recharge, which may also result in ground subsidence or thaw settlement. It should be noted that the lateral groundwater inflow or outflow and the occurrences of snow/rainfall might change with the seasonal weather and anthropogenic activities throughout the whole freeze-thaw period. In addition, dissolved solutes within the soil water may affect heat transfer and hydraulic properties by changing soil freezing characteristics, including freezing point depression. Vapor flow can also affect the heat and mass budget in the unsaturated freezing soil (e.g., Hansson et al., 2004; Huang & Rudolph, 2021). The aforementioned movement of soil water, vapor, heat and solute in variably-saturated deformable soil during a freeze-thaw cycle are closely coupled, nonlinear processes.

2.2. Mathematical Model

In order to simplify the governing equations for water and vapor flow, heat transfer and deformation in unsaturated freezing soil, several basic assumptions are made as follows,

1. The migration of the water and vapor in soil obeys Darcy's law during the freeze-thaw cycles and is driven only by the matric potential, cryosuction and gravity.
2. Soil grains, water and ice are homogeneous, isotropic, and incompressible. Ice growth and expansion are isotropic. The porous soil medium is considered a poroelastic continuum under two-dimensional plane-strain conditions.
3. Water-ice phase change is based on equilibrium thermodynamics and non-hysteretic soil freezing characteristic curves. Pore air pressure in the soil is always equal to atmospheric pressure.
4. Salt (solute) precipitation/dissolution/redistribution processes (e.g., salt crystallization, solute redistribution within soil pores) caused by solute exclusion from the ice phase are negligible. Freezing point depression linearly relates to solute concentration.

2.2.1. Water and Vapor Flow

The general partial differential equation for describing transient water and vapor flow in soils under variably-saturated conditions can be expressed as (e.g., Corapcioglu & Panday, 1995; Philip & De Vries, 1957):

$$\frac{\partial}{\partial t}(\rho_w\theta_w + \rho_i\theta_i + \rho_v\theta_v) = -\nabla\cdot(q_w + q_v) = -\nabla\cdot(\rho_w\boldsymbol{u_w} - D_v\nabla\rho_v) - \rho_w S_w\alpha_b\frac{\partial\varepsilon_{\text{vol}}}{\partial t} \tag{1}$$

where subscripts w, i, and v refer to liquid water, ice and vapor, respectively; ρ is the density (kg $\cdot$ m^{-3}); θ is a volumetric fraction; q is the mass flux (kg $\cdot$ m^{-2} $\cdot$ s^{-1}); t is time (s); S_w is the degree of unfrozen water saturation; D_v is the water vapor diffusivity (m^2 $\cdot$ s^{-1}); ε_{vol} is the volumetric strain of the soil matrix (the sum of the two normal strain components), and α_b is the Biot-Willis coefficient. The thermal-induced liquid water flux related to thermal-hydraulic conduction (Hansson et al., 2004; Noborio et al., 1996; Šimůnek et al., 2018) is neglected in this paper because it has been proven to be much smaller than the water flux driven by the matric potential gradient in practical low-temperature engineering problems (Cui et al., 2020; Zheng et al., 2002). Water density and viscosity are assumed to be constant during a narrow range of temperature changes and solute concentration variations. The effects of solute concentration on water and vapor flow are considered negligible. As such, the pore water velocity (averaged water flux) is calculated as $\boldsymbol{u}_w = -\boldsymbol{K}\nabla(\varphi_h + z)$ based on Darcy's law, where $\boldsymbol{K}$ is the soil hydraulic conductivity tensor (m $\cdot$ s^{-1}) under unsaturated or saturated conditions; φ_h is the soil matric potential or pore-water pressure head (m); z is the elevation (m). Briefly, the terms on the left side of Equation 1 represent the change in volumetric liquid water, ice content, and vapor content, respectively; the terms on the right side represent net liquid and vapor fluxes, and the deformation of pore space (the time rate of expansion of the porous soil matrix), respectively.

The relations between the soil-water characteristic curves and unsaturated hydraulic conductivity are described by the widely used van Genuchten–Mualem constitutive formula (Mualem, 1976; van Genuchten, 1980):

$$S_e = \frac{\theta_w - \theta_r}{\theta_s - \theta_r} = \left(1 + |\alpha\cdot\varphi_h|^n\right)^{-m} \tag{2}$$

$$\boldsymbol{K} = \boldsymbol{K}_s S_e^{0.5}\left[1 - \left(1 - S_e^{1/m}\right)^m\right]^2\cdot 10^{-\xi\theta_i} \tag{3}$$

where S_e is the degree of effective water saturation; θ_s and θ_r are volumetric saturated and residual water content, respectively; α and n are van Genuchten scale and shape parameters relating to the inverse of the air-entry pressure and pore size distribution ($m = 1 - 1/n$), respectively; K_s is the saturated hydraulic conductivity under

non-frozen conditions; ζ is an impedance factor acting as the resistance of ice content to water flow in frozen soil, fixed as seven in this study following Hansson et al. (2004). An empirical equation relating the local porosity to volumetric strain is used to describe the effect of deformation on soil porosity (e.g., Chin et al., 2000; Huang et al., 2022), that is $\phi = 1 - (1 - \phi_0)e^{-\varepsilon_{\mathrm{vol}}}$, where ϕ_0 is the initial soil porosity under non-frozen conditions.

The equivalent vapor content can be expressed as (De Vries, 1958):

$$\theta_v = \rho_v \frac{(\phi - \theta_w)}{\rho_w} = \rho_{\mathrm{vs}} H_r \frac{(\theta_s - \theta_w)}{\rho_w} \tag{4}$$

where the relative humidity is calculated as $H_r = \exp(\varphi_h M_w g/\mathrm{RT})$; M_w is the molecular weight of water (=0.018 kg $\cdot$ mol^{-1}); R is the universal gas constant (=8.341 J $\cdot$ mol^{-1} $\cdot$ K^{-1}); g is the gravitational acceleration (m $\cdot$ s^{-2}); ϕ is the porosity equal to volumetric saturated water content θ_s. The saturated vapor density is a function of temperature T (K), which is given by $\rho_{\mathrm{vs}} = \exp(31.37 - 6{,}014.79T^{-1} - 7.92 \times 10^{-3}T)T^{-1} \times 10^{-3}$ (kg $\cdot$ m^{-3}) (Hillel, 1971). The vapor diffusivity in Equation 1 is calculated by the formula $D_v = D_a\theta_g^{2.5}/\theta_s$, where θ_g is the air-filled porosity (Moldrup et al., 2000); D_a is the diffusivity of water vapor in the air, and it is a function of temperature as $D_a = 2.12 \times 10^{-5} \times (T/273.15)^2$ (m^2 $\cdot$ s^{-1}).

Another primary characteristic of freezing (thawing) soil is cryogenic suction S_c, which can cause significant movement of pore-water from warm to cold regions under uniform pressure fields (e.g., Biermans et al., 1976; Zheng et al., 2002). This thermally-induced driving force usually causes a jump in the migration rate of pore water at every degree Celsius immediately below the freezing point, which can be determined using the Clausius–Clapeyron relation based on equilibrium thermodynamics (Arzanfudi & Al-Khoury, 2018; Huang & Rudolph, 2021):

$$S_c = p_w - p_i = p_w - \rho_i \left(\frac{p_w}{\rho_w} - L_f \ln \frac{T}{T_0} \right) \approx -\rho_i L_f \frac{T_0 - T}{T_0} \tag{5}$$

where p_w is the pore-water pressure (Pa) and p_i is the ice pressure (Pa); T_0 is the freezing/melting point of pure water (=273.15 K); L_f is the latent heat of fusion of water (=3.34 $\times$ 10^5 J $\cdot$ kg^{-1}). By assuming the pressure and temperature are independent driving forces for the pore water flow, the average water flux (Darcy flux) through the soil representative elemental volume is rewritten as:

$$\boldsymbol{u}_w = -\boldsymbol{K} \cdot \left[\nabla(\varphi_h + z) + \frac{\rho_i L_f}{\rho_w g T_f} \nabla T \right] \tag{6}$$

where T_f is the actual freezing point depressed by the existence of dissolved solutes (see Equation 16).

2.2.2. Heat Transfer

According to the energy conservation law and the Fourier heat transfer law based on local thermal equilibrium, the subsurface temperature distribution during the freeze-thaw period can be calculated using the advection-conduction equation, including the transient effects of latent heat of fusion that can be considered a source term (e.g., Tubini et al., 2021) as follows (e.g., De Vries, 1958; Zheng et al., 2002):

$$C_e \frac{\partial T}{\partial t} + L_v \frac{\partial \theta_v}{\partial t} - L_f \rho_i \frac{\partial \theta_i}{\partial t} = \nabla \cdot [\lambda_e \nabla T - C_w T \boldsymbol{u_w} - D_v \nabla \rho_v \cdot (C_v T + L_v)] \tag{7}$$

$$C_e = C_i\theta_i + C_w\theta_w + C_{\mathrm{sg}}\theta_{\mathrm{sg}} + C_a\theta_a \tag{8}$$

$$\lambda_e = \lambda_i^{\theta_i} \lambda_w^{\theta_w} \lambda_{\mathrm{sg}}^{\theta_{\mathrm{sg}}} \lambda_a^{\theta_a} \tag{9}$$

where L_v (J $\cdot$ m^{-3}) is the volumetric latent heat of vaporization of liquid water, which is given by $L_v = L_0\rho_w$, and L_0 (J $\cdot$ kg^{-3}) is the latent heat of vaporization, which can be described as a function of temperature $L_0 = 2.501 \times 10^6 - 2{,}369.2 \times (T - 273.15)$ (Hansson et al., 2004); C_w, C_i, C_a, and C_{sg} are volumetric heat capacities (J $\cdot$ m^{-3} $\cdot$ K^{-1}) of water, ice, air and soil grains, respectively, while λ_w, λ_i, λ_a, and λ_{sg} are their thermal conductivities (W $\cdot$ m^{-1} $\cdot$ K^{-1}), respectively. The equivalent heat capacity of the soil composite C_e is expressed by the arithmetic mean of various constituents, while the equivalent thermal conductivity λ_e is calculated by using the geometric mean. The direct effects of the variations in deformation (small strain) and solute concentration on energy balance are considered minimal and therefore neglected in Equation 7.

2.2.3. Force Equilibrium

Assuming that the inertial terms are negligible, the conservation of momentum for small-strain deformable soil mixtures in the quasi-static state can be expressed as (e.g., Ingebritsen et al., 2006; Lu & Likos, 2004):

$$\nabla \cdot \boldsymbol{\sigma} + \rho_b \boldsymbol{g} = 0 \tag{10}$$

$$\boldsymbol{\varepsilon} = \frac{1}{2}\left[\nabla \mathbf{u} + \nabla \mathbf{u}^T\right] \tag{11}$$

where the tensor $\boldsymbol{\sigma}$ is the total stress tensor; $\mathbf{u}$ is the displacement vector; ρ_b is the soil bulk density (phase-averaged). Note that the stresses and strains here are consistent with the sign that the tension is positive and compression is negative. The relations between stress and strain tensors, including freezing effects, are defined by Hooke-Duhamel's law (e.g., Corapcioglu & Panday, 1995; Huang & Rudolph, 2021; Selvadurai & Suvorov, 2017):

$$\boldsymbol{\sigma} - \boldsymbol{\sigma}_0 = \boldsymbol{C} : (\boldsymbol{\varepsilon} - \boldsymbol{\varepsilon}_0 - \boldsymbol{\varepsilon}_{\text{th}} - \boldsymbol{\varepsilon}_v) - S_w \alpha_b p \boldsymbol{I} \tag{12}$$

$$\boldsymbol{\varepsilon}_v = \frac{(\theta_i + \theta_w - \phi)}{3}\begin{pmatrix} 1+\eta & 1+\eta & 0 \end{pmatrix}^T \tag{13}$$

$$\boldsymbol{\varepsilon}_{\text{th}} = \frac{\omega}{3}\begin{bmatrix} (T - T_{\text{ref}}) & (T - T_{\text{ref}}) & 0 \end{bmatrix}^T \tag{14}$$

where $\boldsymbol{\sigma}_0$ and $\boldsymbol{\varepsilon}_0$ are initial stress and strain, respectively; $\boldsymbol{C}$ is the fourth-order tensor of material stiffness; $\boldsymbol{\varepsilon}_v$ is the ice expansion strain under two-dimensional plane strain condition, where η is Poisson's ratio; $\boldsymbol{\varepsilon}_{\text{th}}$ is the thermal expansion strain, where ω is the thermal expansion coefficient ($=1 \times 10^{-8}\ \text{K}^{-1}$). The expressions for two external strains indicate the equilibrium displacement and stress distribution are calculated in a two-dimensional xz-plane.

2.2.4. Solute Transport

The governing equation describing solute (single species) advective-dispersive transport with a reaction term in the soil is (e.g., Kelleners, 2020; Mohammed et al., 2021):

$$\frac{\partial(\theta_w c + \rho_d K_d c)}{\partial t} = \nabla \cdot [\theta_w \boldsymbol{D}_{\text{mm}} \nabla c - \boldsymbol{u}_w c] + \theta_w r \tag{15}$$

where c is the aqueous concentration of the solute ($\text{mol} \cdot \text{m}^{-3}$, here the dissolved tracer of interest); ρ_d is dry bulk density ($\text{kg} \cdot \text{m}^{-3}$); K_d is physical adsorption coefficient ($\text{m}^3 \cdot \text{kg}^{-1}$); $\boldsymbol{D}_{\text{mm}}$ is the hydrodynamic dispersion tensor ($\text{m}^2 \cdot \text{s}^{-1}$) defining solute spreading by molecular diffusion ($D^* = 5 \times 10^{-11} \times \theta_w$, $\text{m}^2 \cdot \text{s}^{-1}$), where D^* is the diffusion coefficient, and mechanical dispersion through the dispersion coefficient determined by the product of the longitudinal/transverse dispersivity (α_L/α_T, m) and linear fluid velocity; r is a source/sink rate ($\text{mol} \cdot \text{m}^{-3} \cdot \text{s}^{-1}$) due to geochemical reactions such as mineral precipitation/dissolution, ion exchange/complexation, redox reactions, and so on, which are not considered in this study.

2.2.5. Soil Freezing Characteristics

The presence of solutes in unfrozen water and capillary forces can alter the freezing point of the bulk liquid. However, there is not yet a complete consensus regarding the suitable mathematical formulation for their relationships (Williams & Smith, 1989; Zheng et al., 2002). Taking into account the freezing point depression caused by the elevated concentration of the solutes (solutes are excluded from the forming ice leaving the remaining liquid solution more concentrated during the freezing process), a simplified linear relationship is calculated as follows (Liu & Hu, 2017):

$$\rho_w \frac{L_f}{T_0}(T_f - T_0) + \text{RT}_0 c = 0 \tag{16}$$

where T_0 and T_f are the freezing point of the bulk water and solutes-mixed water, respectively. R is the universal gas constant.

The presence of unfrozen water in frozen soil can be described by many empirical and theoretical relationships (e.g., Dall'Amico et al., 2011; Huang & Rudolph, 2022). The soil freezing characteristic curves introduced by Michalowski (1993) have been demonstrated to be flexible enough to describe the variation of the unfrozen water

content with subzero temperature for most soil textures (e.g., Bai et al., 2018; Lein et al., 2019), which can be expressed as,

$$\theta_w = \begin{cases} \theta_0, & T > T_f \\ (\theta_0 - \theta_r)e^{\mu(T-T_f)} + \theta_r, & T \le T_f \end{cases} \tag{17}$$

where θ_0 and θ_r are the initial moisture content of the soil under the non-frozen status before it undergoes freezing and the moisture content (residual moisture) at a low reference temperature where ice content change is negligible, respectively, which can be obtained from test results; μ is an empirical fitting parameter reflecting the transition rate and distribution shape. Following the simplified expression presented by Bai et al. (2018), θ_i is calculated from $\theta_i = (\theta_w - \theta_r) \cdot (1 - S_u)$, where S_u is a normalized saturation degree of the unfrozen water, and is expressed as $S_u = e^{\mu(T-T_f)}$ if $T \le T_f$, and equals 1.0 if $T > T_f$.

2.2.6. Soil–Atmosphere Interface

To simulate real-world conditions as much as possible, we should consider the water-vapor fluxes (e.g., evaporation, precipitation) and heat fluxes (e.g., evaporative heat flux, sensible heat flux) at the interface between the ground surface and atmosphere when defining the top boundary conditions. The evaporation and heat fluxes can be calculated from the surface energy balance equation as follows (van de Griend & Owe, 1994; Šimůnek et al., 2018):

$$L_v E_{\mathrm{sf}} + H_s + G_s - R_n = 0 \tag{18}$$

where the first term is the product of the latent heat of water vaporization (L_v, $\mathrm{J \cdot kg^{-1}}$) and the soil surface evaporation rate (E_{sf}, $\mathrm{kg \cdot m^{-2} \cdot s^{-1}}$); the second term refers to the soil sensible heat flux (H_s, $\mathrm{W \cdot m^{-2}}$); the third refers to the heat flux entering the ground surface (G_s, $\mathrm{W \cdot m^{-2}}$) while the last term represents the net all-wave radiation (R_n, $\mathrm{W \cdot m^{-2}}$). This equation states that all energy received at the Earth's surface is assumed to cool or warm the air above the ground surface (sensible heat flux), the evaporative water (latent heat flux), and the ground surface soil (ground heat flux). If precipitation (rainfall) is considered, the water mass flux into the soil can be expressed as $q_{\mathrm{top}} = \rho_w P - E_{\mathrm{sf}}$, where P refers to the intensity of precipitation ($\mathrm{m \cdot s^{-1}}$) (e.g., Boulet et al., 1997) and q_{top} is the water flux defined as the upper boundary condition.

The formulation used to compute evaporative flux from the bare ground surface is based on a mass transfer approach (Campbell, 1977; van de Griend & Owe, 1994), which is driven by the vapor density difference between the atmosphere and the soil surface:

$$E_{\mathrm{sf}} = \frac{\beta_{\mathrm{sf}} \left(\rho_{\mathrm{vs},z_0} H_{r,z_0} - \rho_{\mathrm{vs},z_{\mathrm{ref}}} H_{r,z_{\mathrm{ref}}} \right)}{r_a} \tag{19}$$

where r_a is the aerodynamic resistance factor ($\mathrm{s \cdot m^{-1}}$) and β_{sf} is the soil resistance factor to water vapor flow; ρ_{vs,z_0} is the saturated vapor density ($\mathrm{kg \cdot m^{-3}}$) at the soil surface z_0(m); $\rho_{\mathrm{vs},z_{\mathrm{ref}}}$ is the saturated vapor density ($\mathrm{kg \cdot m^{-3}}$) in the air at the reference height z_{ref} (2 m used in this study) above the ground surface where air temperature, air humidity, and wind speed are measured; H_{r,z_0} and $H_{r,z_{\mathrm{ref}}}$ are the relative humidity of the atmosphere and soil surface, respectively. The aerodynamic resistance for water vapor flow depends on surface roughness properties and wind speed (Campbell, 1977) and is given by:

$$r_a = \frac{\left[\ln\left(\frac{z_{\mathrm{ref},h} - d}{z_{0h}} \right) - \psi_h \right] \left[\ln\left(\frac{z_{\mathrm{ref},m} - d}{z_{0m}} \right) - \psi_m \right]}{\kappa^2 u_a} \tag{20}$$

where κ is the von Karman constant taken as 0.378, u_a is the wind speed at the reference height ($\mathrm{m \cdot s^{-1}}$), d is the zero-plane displacement height (m) (0 for bare soil), z_{0h} and z_{0m} are the surface roughness length (0.001 m used in this study), $z_{\mathrm{ref},h}$ and $z_{\mathrm{ref},m}$ are the observational heights of specific humidity and wind speed measurement (m), respectively. ψ_h and ψ_m are stability correction factors depending on the atmospheric condition (0 used in this study). More details about these factors can be found in Campbell (1977), van de Griend & Owe (1994), and Zheng et al. (2002). Because soil particles can attract and adsorb water molecules, evaporation from bare ground experiences resistance compared to evaporation from open water. The soil surface resistance of water vapor from

the depth of the evaporative front to the soil surface depends on soil moisture (Merlin et al., 2016). This can be expressed using the linear expression $\beta_{sf} = (\theta_{top} - \theta_r)/(\theta_s - \theta_r)$, where θ_{top} is the soil moisture at the uppermost soil layer. The resistance factor β_{sf} varies with subsurface pressure and soil type ranging between 0 (no evaporation possible) and 1 (no resistance to evaporation).

The sensible heat flux can be calculated as $H_s = C_a(T_s - T_a)/r_a$, where T_s and T_a are the temperature of the soil surface and air near the ground surface, respectively. As such, the heat flux at the ground surface G_s, the upper thermal flux boundary of the model, can be obtained by substituting Equations 19 and 20 into Equation 18 given net radiation R_n. However, the inputs used to calculate R_n not only depend on measurements at the real-world field site but also involve many empirical parameters (e.g., van de Griend & Owe, 1994; Zheng et al., 2002). Another simplified way of representing the upper thermal boundary is only considering the convective heat flux (also known as mixed boundary or Fourier boundary), which is calculated by the following formula (e.g., Arzanfudi & Al-Khoury, 2018; Hansson et al., 2004; Huang et al., 2022):

$$q_T = h_c(T_s - T_a) \tag{21}$$

where h_c is the convective heat transfer coefficient ($W \cdot m^{-2} \cdot K^{-1}$) representing the inverse of the surface resistance to heat exchange by taking into account the interfacial effect between the soil surface and air. This simplified formulation for heat flux across the ground surface was adopted for the current model.

2.3. Numerical Formulation and Implementation

The governing Equations 1, 7, 12 and 15 for the four physical fields (i.e., thermal, hydraulic, mechanical, and concentration fields) are highly nonlinear because their relationships are strongly impacted by each other and coefficients (variables) vary with time and space resulting in a stiffness matrix that is not constant during the freeze-thaw cycles. This coupled system of governing equations along with appropriate initial and boundary conditions within 2D or 3D model domains can be solved by several robust numerical simulators capable of solving nonlinear partial differential equation systems for multiple coupled components such as OpenGeoSys, FEHM, and CODE-BRIGHT (e.g., Winterfeld & Wu, 2020). In the current study, a two-dimensional domain is implicitly solved using the finite element package COMSOL Multiphysics v5.3 (Comsol, 2017). The four governing equations for the plane strain problem can be written in the following general form,

$$d_a \frac{\partial U}{\partial t} + \nabla \cdot \mathbf{\Gamma} = f \tag{22}$$

where U, $\mathbf{\Gamma}$ and f are dependent variables, conservative flux, and source term, respectively, and d_a is a damping or mass coefficient. By applying the backward difference for temporal discretization, the generalized solution of Equation 22 can be given as,

$$\left(d_a \frac{U_\kappa^j - U_\kappa^{j-1}}{\Delta t}, \overline{U}\right)_\Omega - \left(\mathbf{\Gamma}, \nabla\overline{U}\right)_\Omega = \left(f, \overline{U}\right)_\Omega + \left(\boldsymbol{n} \cdot \mathbf{\Gamma}, \overline{U}\right)_{\partial\Omega} \tag{23}$$

where $\overline{U}$ is virtual displacement; $\boldsymbol{n}$ is the outward normal unit vector of a boundary; Ω is the calculation domain; $\partial\Omega$ is the boundary of the calculation domain; the superscript j denotes the time step, and the subscript κ denotes the cell. The resulting system of linearized equations, within each Newton-Raphson iteration, is solved using the Parallel Sparse Direct Solver MUMPS in the fully-coupled (monolithic) approach with a relative tolerance of 1×10^{-6}. A strict implicit backward differentiation formula adaptive time stepping is adopted, and the maximum time step was limited to 0.1 hr. To maintain tradeoffs between computational cost and accuracy, especially for examining the subtle changes in displacement and water vapor flux, a relatively fine triangular 2D mesh (maximum element size 1×10^{-2} m and minimum element size 1×10^{-4} m) was employed for the following numerical experiments. It should be noted that such fine grid spacing could be adjusted depending on the size of the real practical system and the nature of the state variables.

3. Model Verification and Validation

Once the numerical model has been constructed, a confidence assessment must be performed before using it for predictive purposes. This model assessment can demonstrate whether the proposed formulation is capable of

accurately solving the coupled system of governing equations and able to reproduce the main physical processes that occur in the real world. It is usually conducted by comparing the calculated results with analytical solutions, lab/field experimental measurements, and/or simulated results by other proprietary software (e.g., Grenier et al., 2018; McKenzie et al., 2007). In this study, the adopted verification strategy is based on data obtained through two laboratory freeze-thaw tests, in which the experimental observations and numerical simulations are comparably analyzed.

3.1. Laboratory Column Experiments

Column experiments conducted by Wang et al. (2016) and Wu (2017) are used to verify this model. Sieved silica sand with approximately 82% of the material having a particle size distribution of 0.1∼0.25 mm and porosity around 0.39 was used in the Wu (2017) experiments. The upper 30 cm of a 40 cm long Plexiglas cylinder was uniformly packed with preconditioned fine silica sand, and the bottom 10 cm was a liquid reservoir. The whole cylinder was placed into a refrigerator, and the sidewalls were wrapped in 2 cm of rock wool for insulation, except for the top end, which remained open. A 300 mg $\cdot$ L^{-1} KNO_3 solution was added to the cylinder in an amount that ensured the sand would remain partially saturated throughout to monitor how the nitrate migrates during the freezing period. Five 5TE sensors (Decagon Devices INC., USA), with a spacing interval of 5 cm, were placed within the column to record the soil moisture, temperature and electrical conductivity. Prior to the freezing experiment, the temperature within the refrigerator was set at 4°C for at least 24 hr. Once the freezing process was triggered, the temperature within the refrigerator was dropped to, and then kept at, around −10°C, and the bottom water reservoir was maintained at approximately 4°C (one-sided top-down freezing condition) or −10°C (two-sided freezing condition to model a permafrost situation). The freezing tests continued for 36 hr. It should be noted that a direct (in-situ or ex-situ) detection of the dissolved nitrate in the unfrozen soil moisture is extremely challenging because sampling the unfrozen water (moisture), even with a tiny volume, would severely disturb the thermal and hydraulic regime of the cylinder, such that nitrate concentration was inferred from the measured electrical conductivity. The detailed data from one of the two-sided freezing tests were used during the verification stage of the current research although Wu (2017) conducted a series of additional freezing tests using the procedures outlined above.

The procedures of Wang et al. (2016)'s column thaw consolidation experiment were also summarized by Loli et al. (2020). In short, preconditioned silty clay was packed into a set of cylinders of 10 cm in height and diameter. The dry unit weight of soil samples was about 17.5 kN $\cdot$ $m^{-3,}$ and water content was around 0.22 leading to a degree of saturation of 0.6. The downward thaw consolidation of uniformly frozen (at −1°C) samples was triggered by periodically raising the temperature at the top plate. The cylinder was thermally insulated, and the bottom end was kept at −1°C. At the same time, a surcharge load of 100 kPa was applied on the top cap, and a drainage pipe was mounted on the pedestal of the apparatus for free draining. Displacement of the top cap and temperature profiles were monitored by the displacement transducer and five thermal sensors embedded in the wall of the plexiglass cylinder.

3.2. Model Settings and Results

In the Wu (2017) two-sided freezing experiment used for verification purposes, the fine sand was initially unfrozen, and the corresponding numerical model developed to simulate the laboratory results was run to a steady state before freezing started. The temperature at both ends of the column was continuously controlled and monitored during freezing. To get a uniform frozen regime within the soil column, the corresponding numerical model applied to reproduce the Wang et al. (2016) test was initially run to a steady-state under a boundary temperature of −1.0°C. At the start of the thawing process, the upper boundary was set as a temporally varying temperature boundary following $T_{top} = 2.5 + 4\sin(t\pi/3)$ (°C, t denotes time in hours). The bottom boundary was maintained at a constant temperature of −1.0°C during the entire thawing process. The free-draining condition of the upper end was triggered by a boundary load, and cumulative consolidation at the upper boundary was measured during the experiment and calculated with the model. The key parameters used for simulating the freezing and thawing processes within these two column experiments are listed in Table 1.

Figure 2 shows a comparison of the simulated results against measured profiles of the temperature, liquid water (moisture) content, and nitrate concentration. The model's initial conditions agreed with the measured initial

Water Resources Research

10.1029/2022WR032146

Table 1
Parameters Used for Simulating the Freezing and Thawing Processes in Column Experiments by Wang et al. (2016) and Wu (2017), and Performance Evaluation of the Corresponding Model Validation Results

Parameters		Values	
		Wu's (2017) test	Wang et al.'s (2016) test
Hydraulic properties	K_s ($m \cdot s^{-1}$)	2.78×10^{-6}	7.0×10^{-8}
	θ_s ($m^3 \cdot m^{-3}$)	0.39	0.36
	θ_r ($m^3 \cdot m^{-3}$)	0.03	0.05
	α (m^{-1})	2.6	0.65
	n	2.0	1.6
Thermal properties	λ_w ($W \cdot m^{-1} \cdot K^{-1}$)	0.6	0.6
	λ_i ($W \cdot m^{-1} \cdot K^{-1}$)	2.22	2.22
	λ_{sg} ($W \cdot m^{-1} \cdot K^{-1}$)	5.0	2.0
	λ_a ($W \cdot m^{-1} \cdot K^{-1}$)	0.04	0.04
	C_w ($J \cdot m^{-3} \cdot K^{-1}$)	4.18×10^6	4.18×10^6
	C_i ($J \cdot m^{-3} \cdot K^{-1}$)	1.9×10^6	1.9×10^6
	C_{sg} ($J \cdot m^{-3} \cdot K^{-1}$)	1.5×10^6	2.0×10^6
	C_a ($J \cdot m^{-3} \cdot K^{-1}$)	1.23×10^3	1.23×10^3
	μ (K^{-1})	6.0	1.5
Mechanical properties	E (MPa)	–	0.6
	η	–	0.3
	α_b	–	1.0
Transport properties	α_L (m)	5.0	–
	α_T (m)	0.1	–
	K_d ($m^3 \cdot kg^{-1}$)	3.0×10^{-5}	–

	Indices	Temp. (°C)	Water cont. ($m^3 \cdot m^{-3}$)	Nitrate conc. (g/L)	Temp. (°C)	Deformation (mm)
Model's fitting performance	r	0.992	0.965	0.791	0.989	0.985
	E_{NS}	0.989	0.932	0.535	0.949	0.939

Note. r denotes Pearson correlation coefficient and E_{NS} refers to Nash–Sutcliffe model fitting efficiency coefficient.

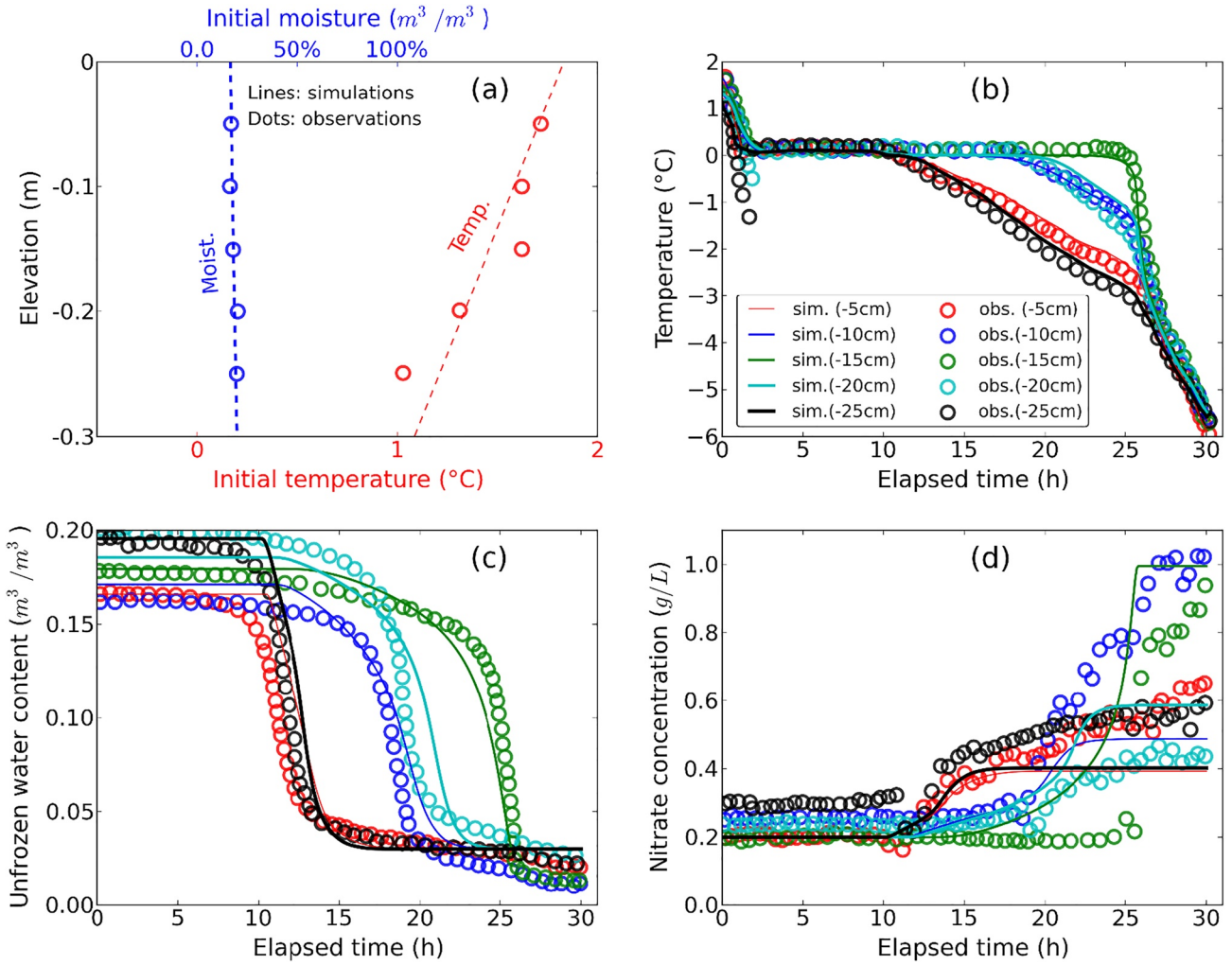

Figure 2. (a) The initial temperature and initial moisture content, (b) transient temperature profiles, (c) moisture content profiles and (d) nitrate concentration profiles in laboratory freezing experiment (dots) by Wu (2017) compared to the corresponding numerical simulation results (lines).

temperatures and soil water contents as illustrated in Figure 2a. The Pearson correlation coefficient and Nash–Sutcliffe coefficient are both higher than 0.98 in Table 1, indicating that the predicted values of temperature agree very well with the measured ones (Figure 2b). There were some minor differences between the simulated results and observations of the unfrozen water content (Figure 2c). However, in general, the rapid decrease of total water content in the freezing front is well reproduced. In terms of the nitrate concentration, the simulated results were not in as good agreement with the measured data, particularly at a later time, although they generally shared similar trends (Figure 2d). The Pearson correlation coefficient and Nash–Sutcliffe coefficient are 0.791 and 0.535, respectively, suggesting a significant degree of deviation between the simulations and the laboratory measurements. These discrepancies need further examination but may be due to the uncertainty of the model structure, such as neglecting the influence of soil heterogeneity or preferential flow paths, and the data collection approach that may have involved conversion errors from electrical conductivity and the averaging characteristics of the probes (Wu, 2017).

Comparisons between the observed temperature profiles and deformation of the top plate from the Wang et al. (2016) column test and the simulated results are presented in Figure 3. The simulated soil temperature profiles were in very good agreement with experimental observations (Figure 3a). The step-pattern curve of thaw and refreeze deformation in Figure 3b shows that the simulation results slightly deviate from the measured data, especially during the latter period, which might be related to the weakness of assuming a linear poroelasticity for frozen soils in our numerical model. For example, the phenomenon of frost heave is insignificant in

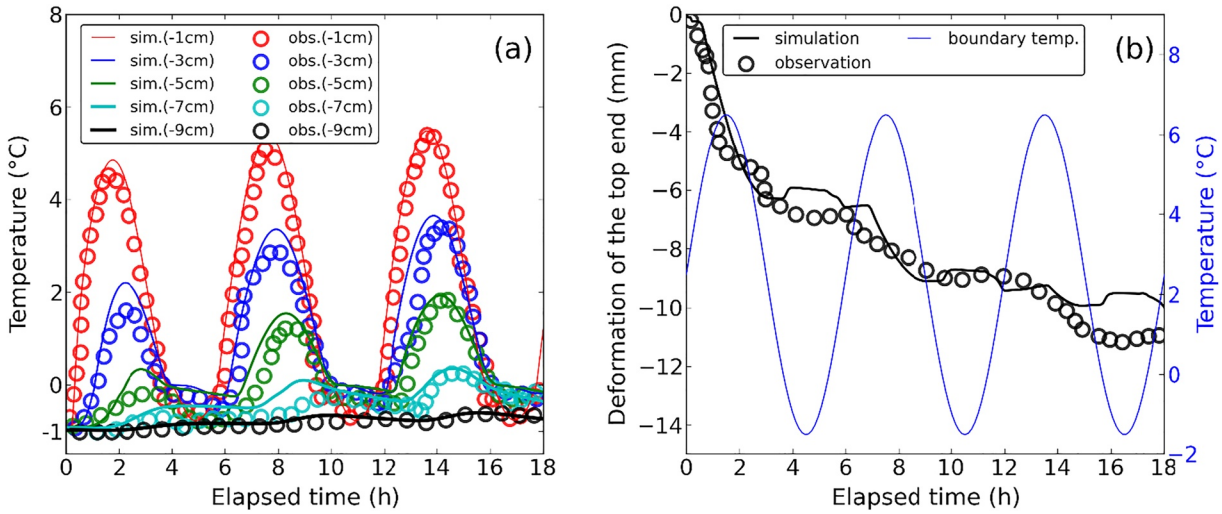

Figure 3. (a) The transient temperature profiles and (b) deformation history documented during the laboratory freeze-thaw experiment (dots) by Wang et al. (2016) compared to the corresponding numerical simulation results (lines).

the experimental observations when the top boundary temperature is below 0°C, which shows a probability of non-elastic soil deformation and requires further examination. As shown in Table 1, the Pearson correlation coefficient and Nash–Sutcliffe coefficient are all higher than 0.9. In general, the trends of thaw-induced deformation (settlement) and freeze-induced frost heave were well captured by the simulations.

Collectively, according to the acceptable agreement between the experimental data from the literature and the simulated profiles of temperature, water content and deformation, our proposed THM-C coupling model appears to reasonably represent the transient mechanisms of heat-moisture-deformation in variably-saturated freezing soil.

4. Heat and Mass Transfer in Deformable Variably-Saturated Freezing Soils

Utilizing the proposed model, a numerical analysis of water and vapor flow, heat transfer, frost heave and thaw settlement, and solute transport during periodic freeze-thaw cycles is presented for various soil types. We examine the diurnal forcing of warm temperatures during the days (6°C) and freezing temperatures during the nights (−4°C) at the beginning of the winter period to predict how the different soil textures respond. The selected three soil textures are sand, clay and silt (i.e., USDA soil textural classification), which are typical soil types encountered in glacial terrain and shallow permafrost active layers within cold climate environments. Three typical soil transect profiles, each 1.0 m deep and 2 m wide, are specific for the simulations, and their parameters are listed in Table 2. The transect model is a two-dimensional domain along the ground surface (x) and vertical (z) gravity directions. The boundary and the initial conditions are determined according to the practical engineering conditions that would prevail in cold and semi-arid regions (e.g., Williams & Smith, 1989; Zhang et al., 2016). The bottom and both sides are designed as no-flow (water and solute) and roller boundaries (displacement) (see Figure S1 in Supporting Information S1). At the same time, the top boundary is mechanically free and driven by a variable heat flux (Equation 21) with a periodic changing air temperature $T_a = 5\sin\left(\frac{2\pi}{24}t\right) + 1$ (°C, the freeze-thaw period is 24 hr following Yu et al., 2020) and a constant heat transfer coefficient $h_c = 28\ \mathrm{W \cdot m^{-2} \cdot K^{-1}}$ (following Hansson et al., 2004). No natural external precipitation incident at the ground surface is considered for the scenarios, which means $q_{\mathrm{top}} = -E_{\mathrm{sf}}$. Thus, only evaporation and heat flow are allowed on the top boundary. The temperature at the bottom boundary is considered as groundwater temperature and kept at 1.0°C, while both sides are designed as heat insulating. It should be noted that although the computational system is 2D in this study, the processes of heat transfer, water flow and solute transport are essentially simulated as a simple 1D system with the adopted boundary conditions.

The initial temperature throughout the domain before the surface temperature cycling commences is 1.0°C. The initial water content and soil thermal properties are predicted under a gravity-drained condition with

Table 2
The Hydraulic, Thermal, Mechanical and Chemical Properties for Three Typical Soil Textures Compiled From Carsel and Parrish (1988), Chung and Horton (1987), Oke (2002), Serne (2007), Williams and Smith (1989), and Zhang et al. (2016) (Baseline Case S0)

Parameter		Sand	Silt	Clay
Hydraulic properties	K_s ($m \cdot s^{-1}$)	8.25×10^{-5}	2.55×10^{-6}	5.6×10^{-7}
	θ_s ($m^3 \cdot m^{-3}$)	0.43	0.49	0.38
	θ_r ($m^3 \cdot m^{-3}$)	0.045	0.065	0.068
	α (m^{-1})	14.5	0.55	0.8
	n	2.68	2.32	1.09
Thermal properties	λ_{sg} ($W \cdot m^{-1} \cdot K^{-1}$)	5.5	3.5	1.5
	C_{sg} ($J \cdot m^{-3} \cdot K^{-1}$)	2.1×10^6	2.3×10^6	2.5×10^6
	μ (K^{-1})	2.0	0.6	0.2
Mechanical properties	E (MPa)	5.0	2.5	1.0
	η	0.3	0.3	0.3
	α_b	1.0	1.0	1.0
Transport properties	α_L (m)	0.5	0.5	0.5
	α_T (m)	0.05	0.05	0.05
	K_d ($m^3 \cdot kg^{-1}$)	5.0×10^{-4}	5.0×10^{-4}	5.0×10^{-4}

the groundwater table set at −0.6 m (pressure head at the bottom boundary is therefore 0.4 m), as shown in Figures 4a–4c. The selected soil hydraulic and thermal properties against temperatures are shown in Figures 4d–4f and Figure S2 in Supporting Information S1. The initial concentration of tracer throughout each soil layer is a uniform 1.0 mmol $\cdot L^{-1,}$ and no other external solute sources are included. The in-situ stress state is geostatic with gravity under plane-strain conditions. Before the periodic freeze-thaw action starts, all models are run to be at steady-state (spin-up procedures) to achieve a stable initial condition for the subsequent transient simulations. For model assessment and illustrative purposes, the simulation results of vertical soil profiles in the middle of the 2D transect model domain (at $x = 0$ m in Figure S1 in Supporting Information S1) during a 5-day freeze-thaw sequence (e.g., Yu et al., 2020) are presented and analyzed. The simulation scenario designed for the numerical experimentation is intended to represent a short-term diurnal freezing and thawing cycle that would allow for the examination of the main processes occurring in seasonally frozen areas and the active layers of permafrost regions in a computationally efficient manner. The depth of the simulation domain was selected to capture the vertical variations in the subsurface when exposed to a daily freezing and thawing sequence over the 5-day period. Depending on the spatial and temporal scale of the problem of interest, the model can be scaled-up to represent the boundary conditions and time frames of interest.

Figure 5 presents the numerical results for three typical soil layers, which are initially in an unfrozen state before the freeze-thaw cycling starts. The temperatures imposed on the upper (transient) and lower (constant) boundaries are shown in Figure 5a. When air temperature is below the freezing point, the freezing front advances downward, as shown in Figure 5b. However, the period when the maximum frost depth appears does not correspond to the coldest air temperature but lags for a couple of hours. The advancing rate of the freezing front in the sand is the fastest and results in the highest maximum frost depth, followed by the clay, while the freezing front in silt advances the slowest, resulting in the shallowest frost depth penetration. This is due to more ice formation in the silt relative to the other soil types, which releases a larger amount of latent heat, which buffers the cold temperature (e.g., Huang & Rudolph, 2021). In addition, there is an intense periodical fluctuation of the water table in the silt, a slight fluctuation of the water table in the clay, and almost no groundwater level change in the sand. The changing heat capacity of porous soil medium and flow velocity in space and time are shown in Figure S3 in Supporting Information S1.

During the freezing stage, the magnitude of water table drawdown in the silt and clay soils is related to the amount of water that migrates upward to the unsaturated zone from the underlying saturated porous media as a result of the cryogenic suction process (Figure 5c). This process is illustrated by the water flux calculations shown in

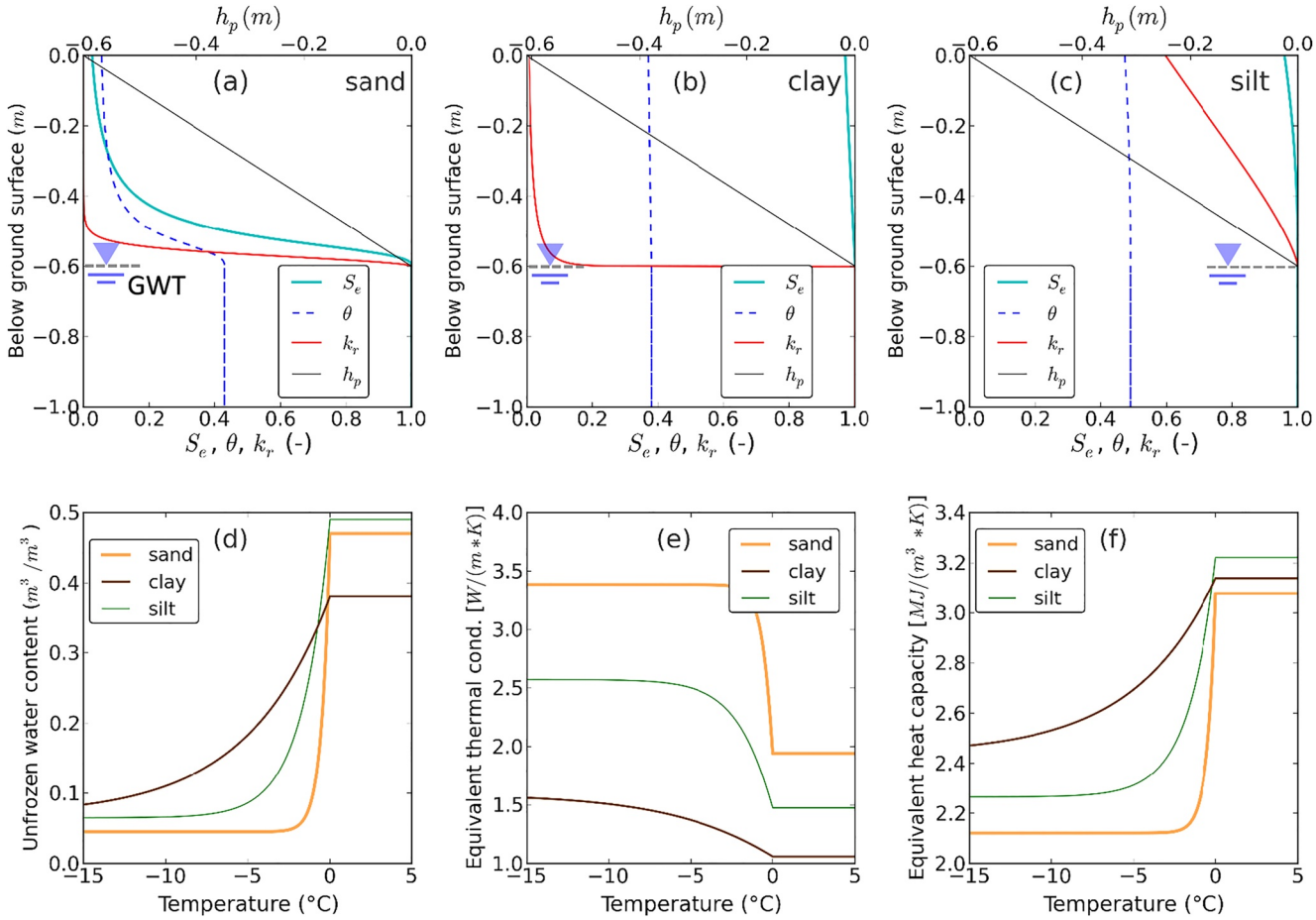

Figure 4. The initial distribution of the relative degree of saturation (S_e), water content (Θ), relative hydraulic conductivity (k_r), and pressure head (h_p) under a drained condition with the average groundwater table (GWT) depth at −0.6 m for three typical soil textural classes, sand (a), clay (b), and silt (c), respectively. Variation of the unfrozen water content (d), equivalent thermal conductivity (e), and equivalent heat capacity (f) with temperature for those three typical soil textures under saturated conditions. Parameters used for these predictions are given in Table 2.

Figures 7a and 8a. Freezing of the accumulated water (moisture) will expand the pore space and may result in a frost heave. For example, positive displacements are simulated in the upper silt layer, while negative displacements are predicted in the unfrozen zone and deep part of the frozen zone (Figure 5d). This phenomenon of negative displacement has been reported by others in the past (e.g., Huang & Rudolph, 2021; Tiedje & Guo, 2011), and is interpreted to be due to the rapid dewatering ahead of the freezing front and an increase of soil unit weight in the frozen zone cause considerable frost-induced volume shrinkage. During the thawing stage, the frozen zone is thinned progressively as the thawing front advances until it disappears. A small part of the thawed excess pore water will be evaporated while the remaining fraction will infiltrate downwards under the action of gravity resulting in some recovery of groundwater levels (Figure 5c). The deformation in the soil profile that results from the freezing process gradually disappears during the thaw cycle as the released water migrates back downward (water loss zone) (Figures 5c and 5d).

Figure 5e shows the spatiotemporal variation of the conservative tracer concentration. It can be seen that solute transport from the unfrozen zone to the upper silt layer is much more significant than that in clay and sand. The differences in such solute transport are mainly caused by the different water fluxes in the different soil types. To further explore the dynamic changes that occur in the freeze-thaw zone, the temporal variations of typical state variables at the ground surface ($z = 0.0$ cm) and below the ground surface ($z = -1.0$ cm) within the three different soil layers are discussed in the following two paragraphs, respectively.

Figure 6a shows that the simulated heat flux at the ground surface of the silt soil layer exhibits the largest variations (−200∼200 W · m^{-2}), although they all share a sinusoidal changing trend. The heat flux in the sand layer

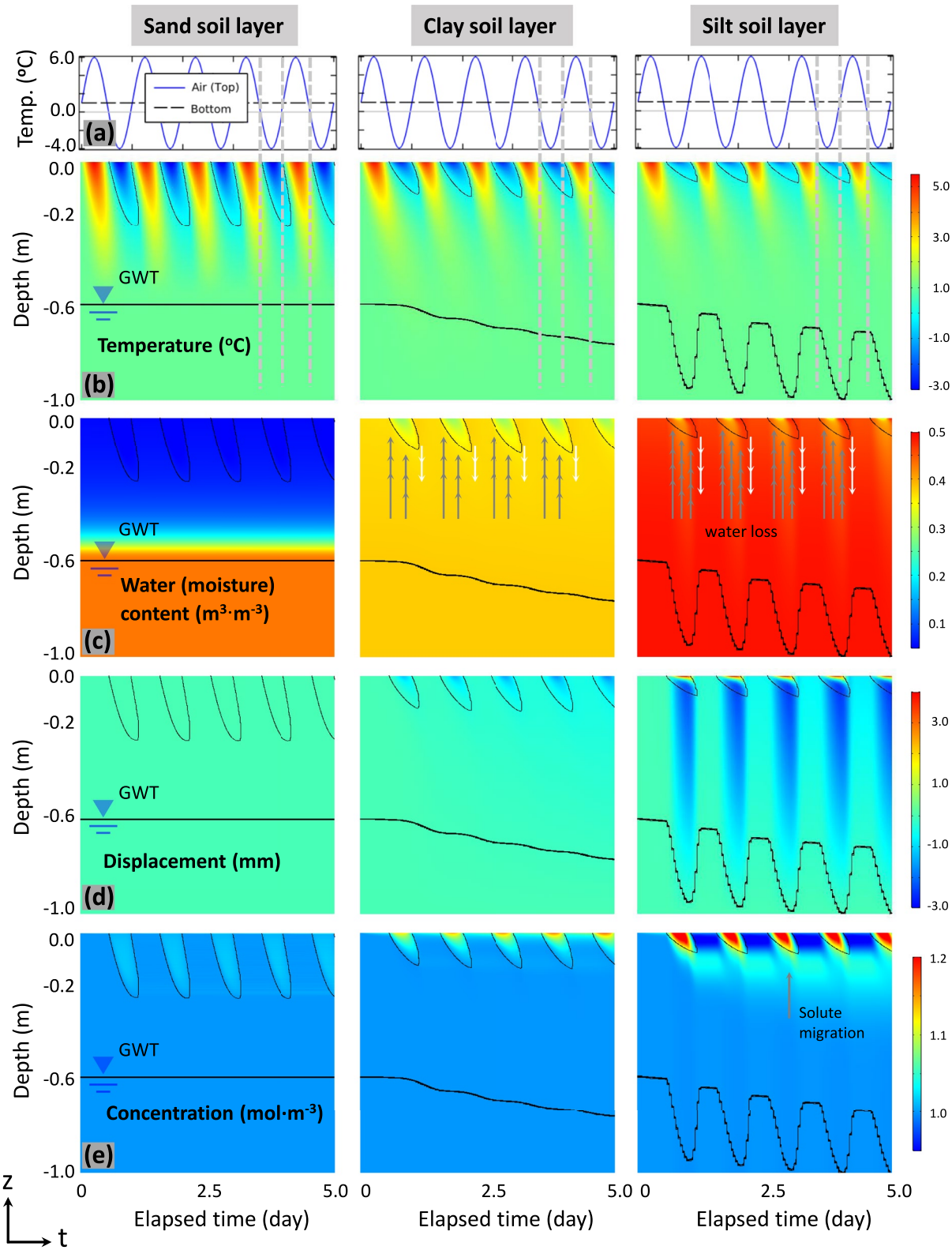

Figure 5. Freeze-thaw cycling on an initially unfrozen sand (left column), clay (middle column) and silt (right column) soil layers. From top to bottom, panels are (a) top and bottom temperature boundary conditions, (b) thermal regime, (c) water (moisture) content evolution (arrow lines indicate the flow vector), (d) displacement history, and (e) tracer (conservative) concentration variation along the middle of 2D transect model domain at $x = 0$, respectively. The thin and thick black lines refer to the freezing front and groundwater table, respectively.

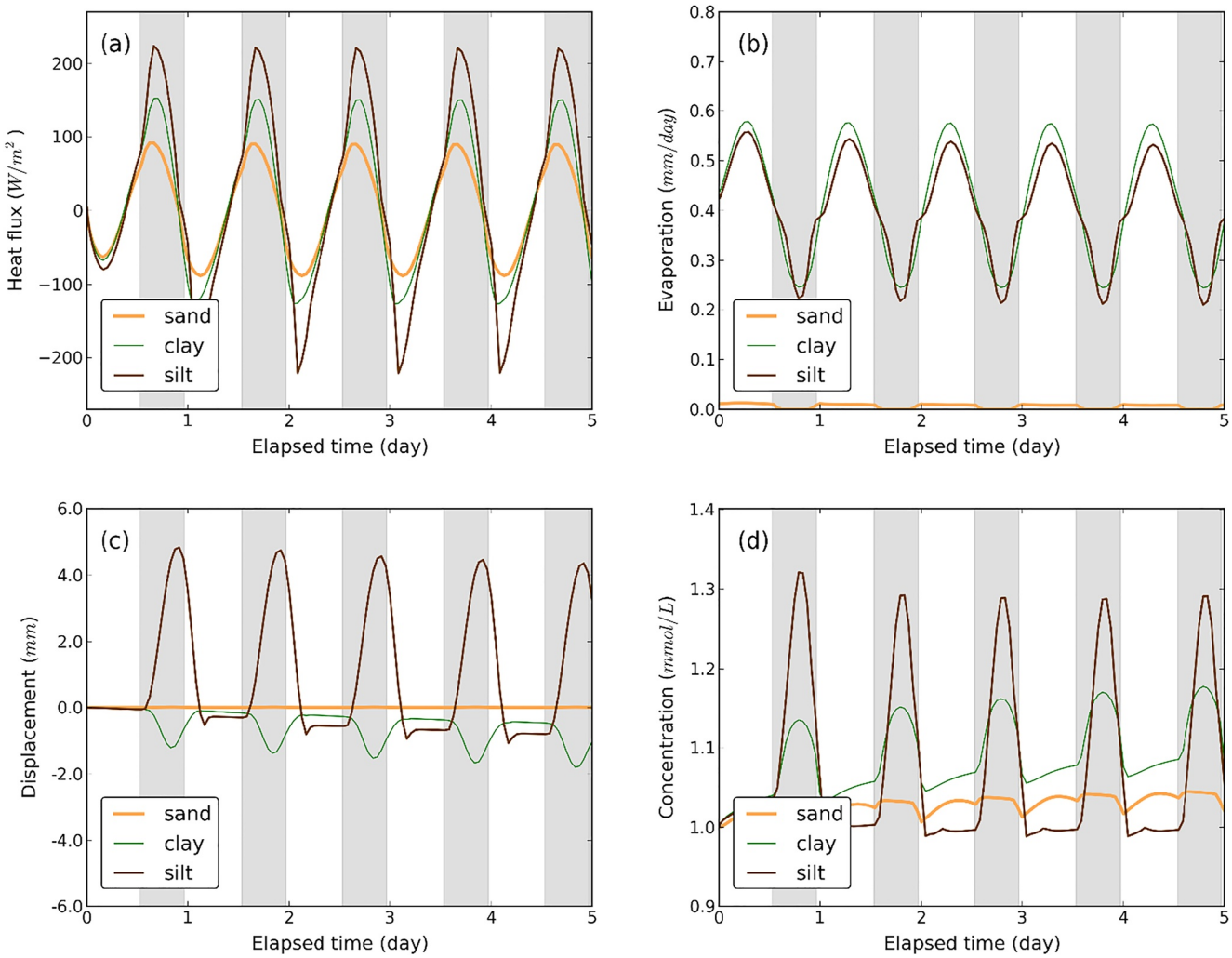

Figure 6. The evolution of simulated (a) heat flux, (b) evaporation rate, (c) displacement and (d) tracer concentration at the ground surface (top-end of model domain) for the sand, clay and silt soil layers. The gray shadow zones delineate the freezing stage and the others refer to the non-freezing period.

is mainly controlled by heat conduction rather than advection because of the low evaporation rate, as shown in Figure 6b. The sand layer's evaporation rate is minimal due to its low moisture content, while the clay and silt share almost the same evaporation pattern. This pattern is also similar to the periodic changing of air temperature. Considering the ground surface deformation illustrated in Figure 6c, there is a competition between the frost heave above the freezing front and the frost-induced volume shrinkage (consolidation) below the freezing front (e.g., Figure 5d). The largest net frost heave in the silt reaches approximately 5.0 mm while the maximum settlement in clay is around 1.0 mm, whose occurrences in the freezing stage need further examination. Here it should be noted that the magnitude of the displacement depends on soil textures and the nature of the forcing function. After 5 days of the diurnal freeze-thaw cycling, there is a slight amount of subsidence at the ground surface of the silt and clay soils, which is likely due to more significant dewatering due to evaporation from the silt and clay. According to Figure 6d, the solute concentration variation at the upper boundary is distinct for the three soil types. The largest magnitude and fluctuation occur in the silt, followed by the clay. Only minor variations are predicted in the sand soils. It is interesting to notice a decrease in solute concentration in the top-ground surface of the silt and clay layers during the thawing period. This is due to the local dilution caused by water being released during the thawing process that results in a lower solute concentration.

Figure 7 presents the simulation results at the location of −0.01 m (below ground surface) in the three soil layers. During the freezing period, the highest flux of liquid water between the unfrozen zone and the frozen zone occurs in the silt, followed by the clay (Figure 7a). The water flux reaches a maximum during the freezing period and

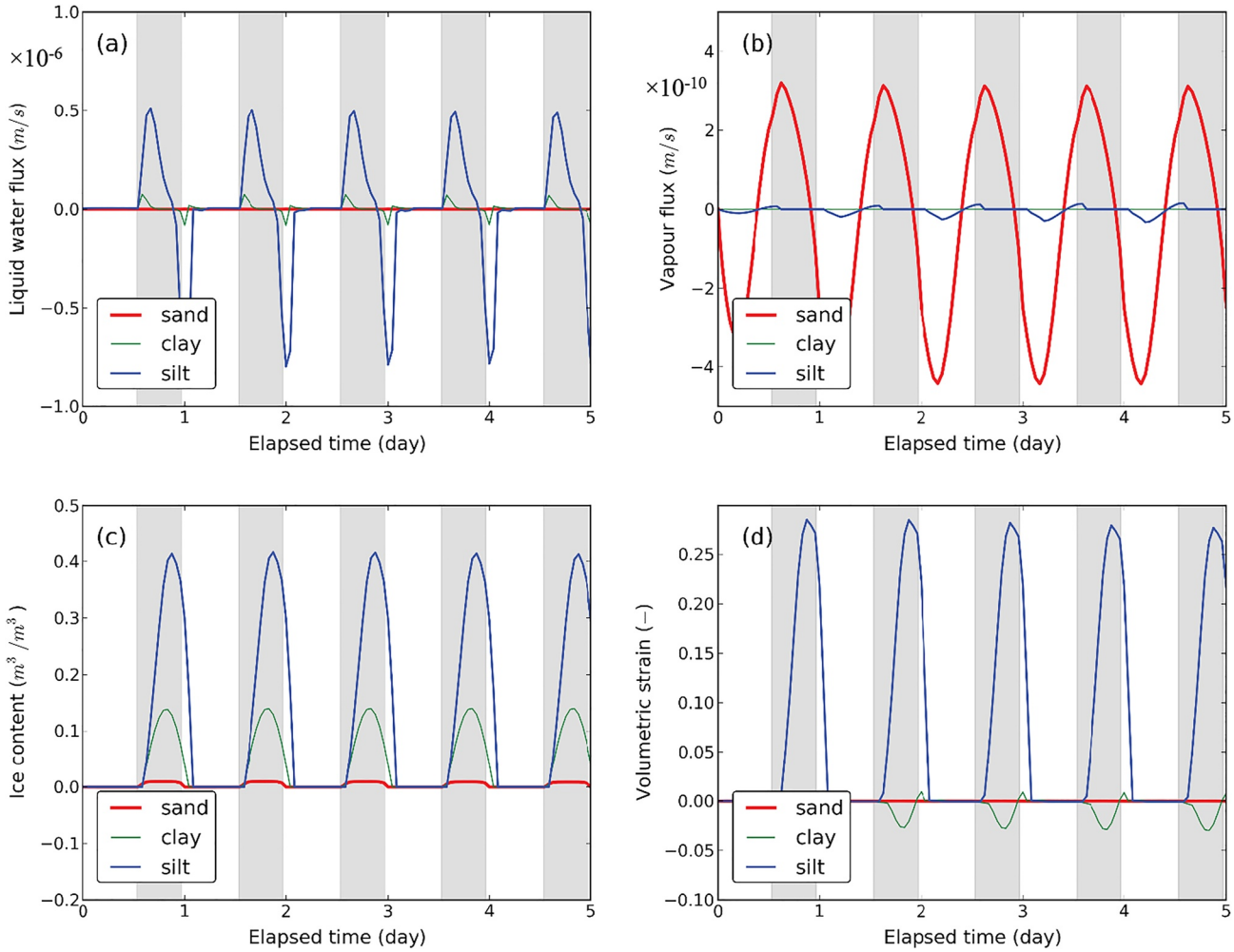

Figure 7. The evolution of simulated (a) liquid water flux, (b) vapor flux, (c) ice content and (d) volumetric strain at the location (−0.01 m) immediately below the ground surface in the sand, clay and silt soil layers. The gray shadow zones delineate the freezing stage and the others refer to the non-freezing period.

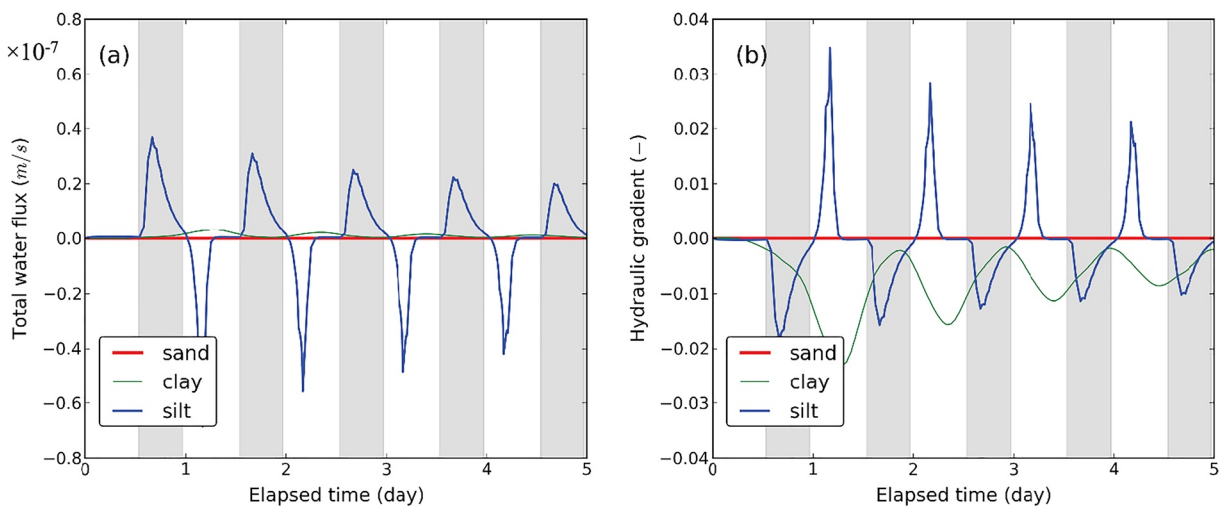

Figure 8. The evolution of simulated (a) total water flux and (b) hydraulic gradient at the groundwater table in the sand, clay and silt soil layers. The gray shadow zones delineate the freezing stage and the others refer to the non-freezing period.

Table 3
Key Details and Differences in Simulation Scenarios

Scenario	FT period (day)	Amplitude (°C)	Hydraulic cond.	Initial GWT (m)	Initial conc. (mmol · L^{-1})	Dispersiv. (α_L, m)	Adsorption
S0	1.0	5.0	K_s	−0.6	1.0	0.5	Yes
S1a	2.0	5.0	K_s	−0.6	1.0	0.5	Yes
S1b	1.0	8.0	K_s	−0.6	1.0	0.5	Yes
S2a	1.0	5.0	$K_s \times 5$	−0.6	1.0	0.5	Yes
S2b	1.0	5.0	$K_s \times 0.2$	−0.6	1.0	0.5	Yes
S3a	1.0	5.0	K_s	−0.4	1.0	0.5	Yes
S3b	1.0	5.0	K_s	−0.8	1.0	0.5	Yes
S4a	1.0	5.0	K_s	−0.6	100	5.0	Yes
S4b	1.0	5.0	K_s	−0.6	100	0.05	Yes
S4c	1.0	5.0	K_s	−0.6	100	0.05	No

Note. FT and GWT refer to freeze-thaw and groundwater table, respectively. Because the solute concentration in S0 is relatively low, resulting in a very small effect on the freezing point, it can still be regarded as a baseline scenario that is barely impacted by the variation of solute concentration or without considering freezing point depression.

begins to decline, reversing dramatically when the thaw period begins. The liquid water flow in the sand is negligible. However, substantial vapor flow occurs in the sand (Figure 7b), while very small vapor flux occurs in the silt and is insignificant in the clay as a result of the high soil water contents in these two soil types. This finding indicates the vapor flux is non-negligible in the sand, consistent with the observations of Zhang et al. (2016) suggesting that water vapor can transfer water toward the freezing front in the fairly dry sand, although this process appears to contribute only a small percentage of ice content (Figure 7c). Figure 7c also illustrates that the high ice content in the silt over one freezing stage results in significant frost heave (e.g., Figures 5d and 6c) because of the high water flux (Figure 7a). At the same time, there is a substantial expansion of the pore space in the silt and slight volume shrinkage in the clay, as shown in Figure 7d.

The impacts of freeze-thaw cycling on the groundwater dynamics in different soil textures can be examined by comparing the pore water flow velocity and hydraulic gradient at the moving groundwater table. Figure 8a shows that the variation of total water flux (liquid water and vapor) at the groundwater table is similar to the pattern of liquid water flux at the location immediately below the ground surface in the freeze-thaw zone in Figure 7a, except for a short time lag during the thawing stage. In the clay layer, this lag is much more significant (Figure 8a). The clay and silt soils have somewhat opposite responses during the freezing and thaw stages, and the silt is more dynamic with much higher magnitudes of water flux and hydraulic gradient (Figure 8b). The water table in the sand does not respond at all as noted earlier.

5. Analysis of the Effects of State Variables and External Drivers on Soil Freeze-Thaw Processes

To evaluate the influence of several key boundary conditions and state variables on soil behavior during freeze-thaw cycles, we conducted a series of parametric analyses based on a set of different freezing and thawing scenarios for the three soil types selected for this study. Although many factors may affect the coupled heat-moisture-deformation-solute transport processes during the freeze-thaw process, we conduct a single-variable sensitivity analysis for each scenario focusing on several of the most sensitive factors. The baseline scenario S0 refers to the simulations in Section 4 and Table 3 lists the key details and differences between the simulation scenarios.

5.1. Effect of Air Temperature

Two scenarios are designed to reflect the changes in air temperature near the ground surface, which is one of the crucial meteorological variables driving the freeze-thaw cycles. The sinusoidal freeze-thaw period in scenario S1a (2 days) is extended to be twice as long as that in the base case scenario S0 (1 day, which was the cycle period

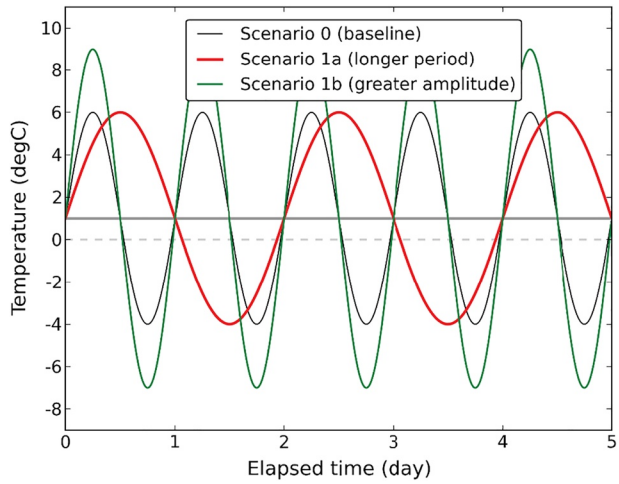

Figure 9. Air temperatures with periodic varying patterns are designed as the top thermal boundary for scenarios S0, S1a, and S1b. The thick gray line refers to the bottom temperature boundary with 1°C.

utilized in the model performance evaluation above). The temperature amplitude is increased by 3°C (9°C during the day and −7°C at night) in scenario S1b for a 1-day period, as shown in Figure 9. The other model domain settings are kept the same as those in the baseline scenario in Section 4. As illustrated in Figure 10a, the greater amplitude and more extended freezing period can lead to a deeper freezing front for the same soil layer. Even under the more extreme freezing conditions, no fluctuation of the water table is observed in the sand, and only very minor variations are noted for the clay. The influence is much more significant in the silt. Similarly, Figure 10b shows that the frost-induced volume shrinkage (consolidation) ahead of the freezing front in clay and the frost heave above the freezing front in silt are also more extensive with the increasing amplitude of air temperature oscillation and the increasing period of freeze-thaw cycles. According to the simulated results in Figure 10c, the concentration profile in silt is the most sensitive to changes in air temperature. More specifically, the peak concentration in the silt over one freezing stage increases with greater amplitude and a more extended freeze-thaw period. A similar trend is also seen in clay albeit at a much lower magnitude and the effect in the sand was negligible.

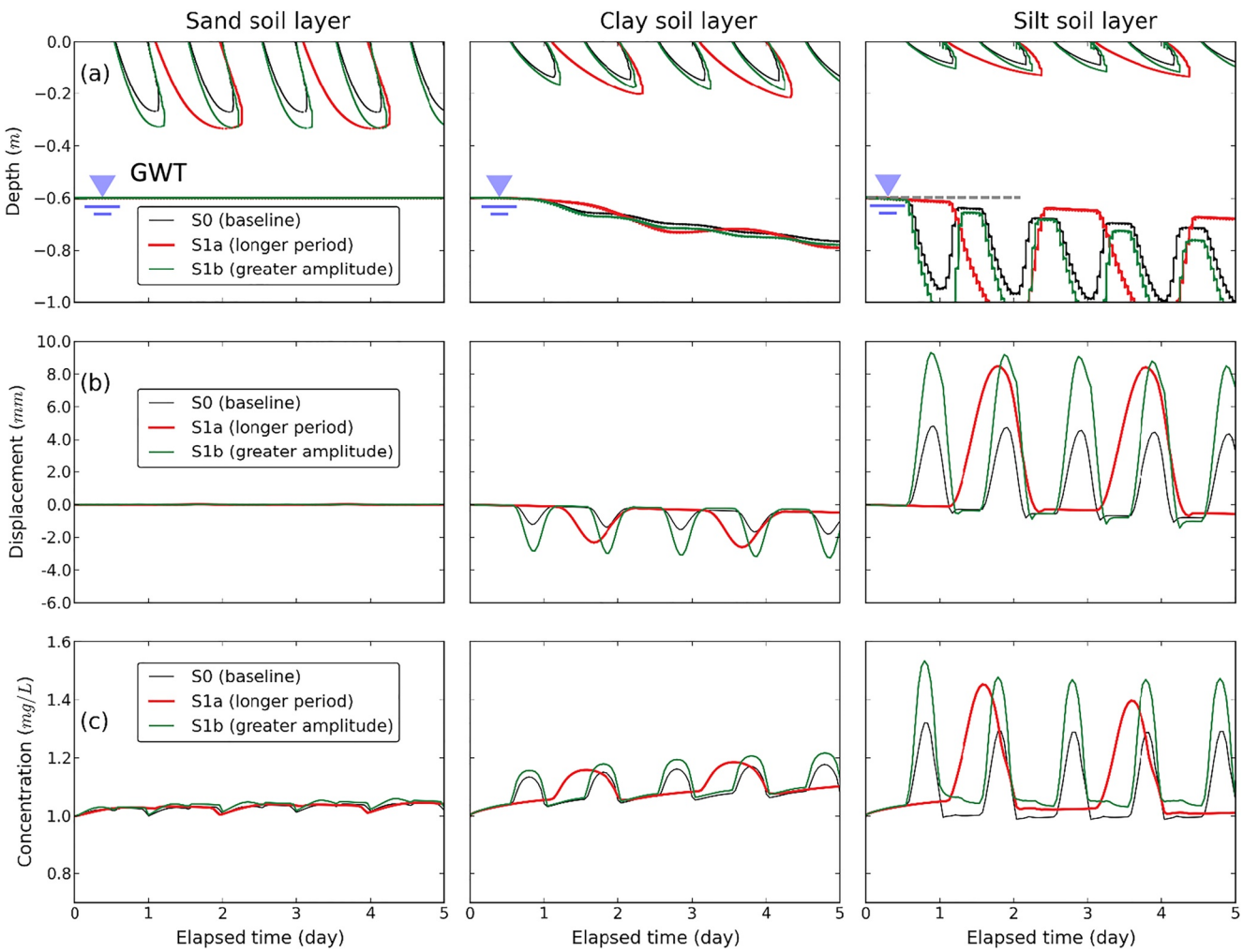

Figure 10. The effect of changing air temperature on freeze-thaw processes in the sand, clay and silt soil layers. From top to bottom panels are (a) freezing front and groundwater table, (b) displacement, and (c) tracer concentration evolution at the ground surface (top-end of the model domain), respectively.

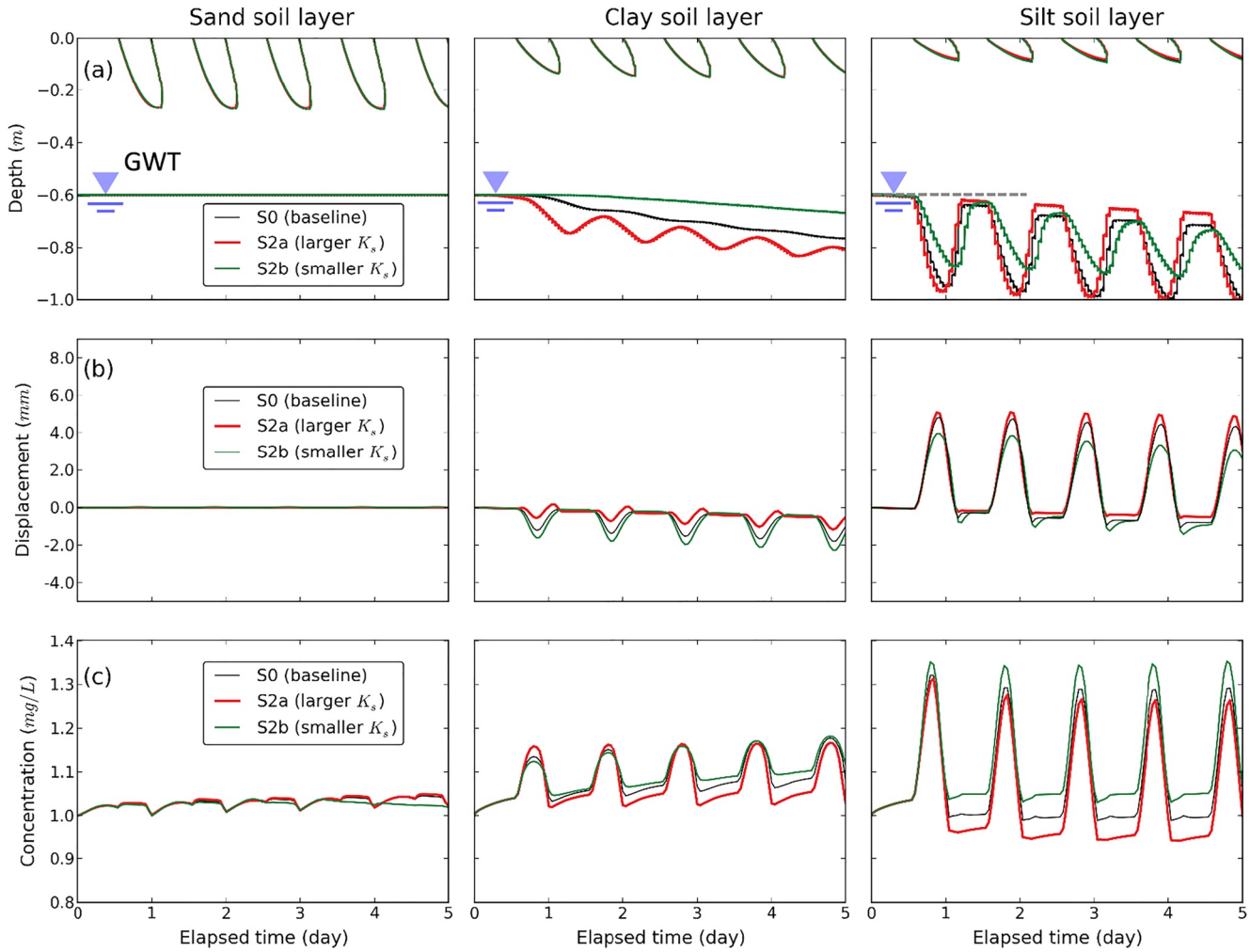

Figure 11. The effect of changing hydraulic conductivity on freeze-thaw processes in the sand, clay and silt soil layers. From top to bottom panels are (a) freezing front and groundwater table, (b) displacement, and (c) tracer concentration evolution at the ground surface (top-end of the model domain), respectively.

5.2. Effect of Hydraulic Conductivity

Soil water (moisture) movement is controlled by hydraulic gradient and hydraulic conductivity. Natural variations in hydraulic conductivity can significantly affect water flow in frozen soil (e.g., Williams & Smith, 1989; Zheng et al., 2002). In this numerical experiment, two scenarios with different values of the intrinsic hydraulic conductivity were analyzed, which are five times larger K_0 in scenario S2a and five times smaller K_0 in scenario S2b in comparison to the baseline values in S0. Figure 11a illustrates that higher hydraulic conductivity values result in more noticeable fluctuation and depression of the groundwater table during the freeze-thaw cycles in the clay and silt, while the water table depth remains unchanged in the sand. This is due to the increase in the flow rate of soil water moving toward or away from the freezing front with higher hydraulic conductivity. As more soil water migrates upward to replenish the water loss zone, it may accumulate near the freezing front resulting in less volume shrinkage (consolidation) and more frost heave of the clay and silt soil layers during the freezing stage, as shown in Figure 11b. The solute transport was also impacted by the variations in hydraulic conductivity in Figure 11c, although no significant trend was found, and further experimental research is needed.

5.3. Effect of Initial Groundwater Table Depth

The initial water (moisture) content distribution and groundwater table depth affect the total water storage in each soil layer, controlling the amount of water that can participate in the freeze-thaw processes. Because the initial water content is calculated by running the model to steady-state (gravity drained condition), we only need to focus

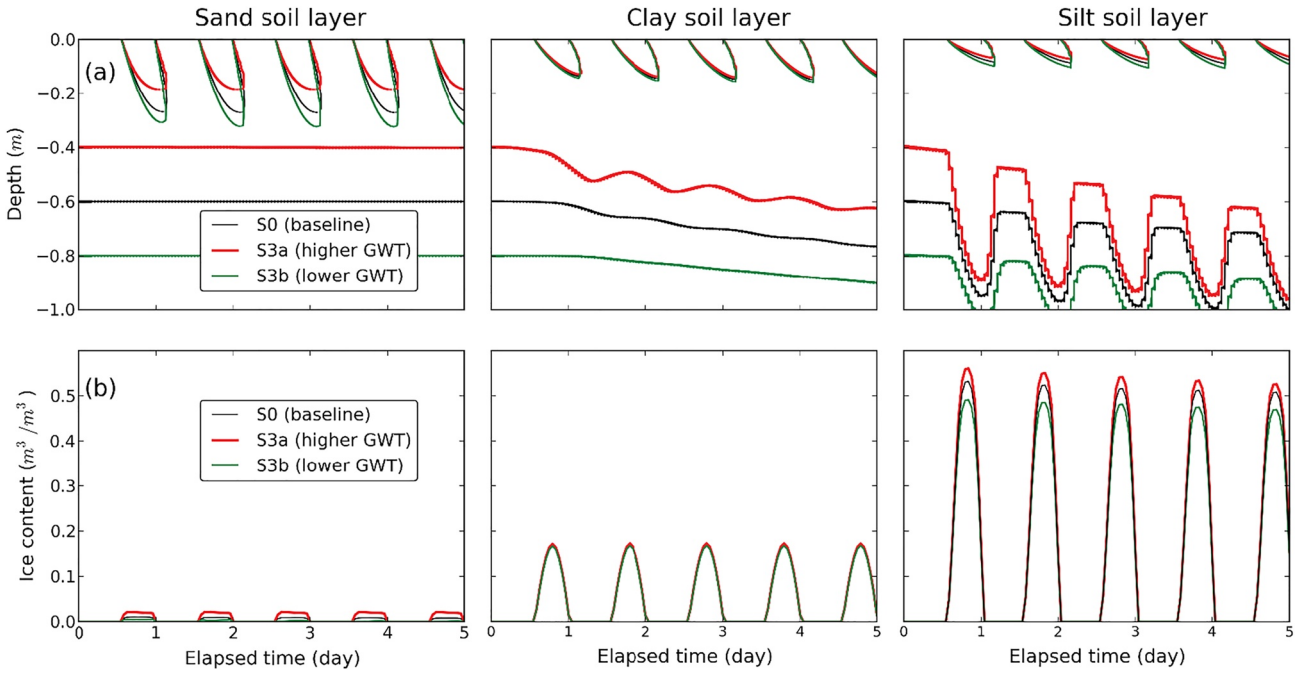

Figure 12. The effect of different initial groundwater levels on freeze-thaw processes in the sand, clay and silt soil layers. The top and bottom panels show (a) the freezing front and groundwater table and (b) volumetric ice content at the ground surface (top-end of the model domain), respectively.

on different depths of the initial groundwater table. Therefore, two additional scenarios are designed: the groundwater level in scenarios S3a and S3b are −0.4 and −0.8 m, respectively, and the groundwater level in the base case S0, remains at −0.6 m. All other simulation conditions are the same as those in Section 4. Figure 12a illustrates the transient evolution of the freezing front and water table in three soil types. It can be seen that the penetration curve of the freezing front in the sand is the most sensitive to the initial depth of the groundwater table, although groundwater levels are flat during the entire freeze-thaw period. By contrast, there are significant fluctuations in the groundwater table and slight changes in the pattern of the freezing front in the silt. The shape of the freezing front penetration curve in clay is less sensitive to different depths of the initial water table because of the very low permeability and thick capillary fringe of the clay. In addition, the intensity of groundwater level oscillations fades with increasing water table depth in the clay soil. Figure 12b illustrates that the ice content increases slightly with the elevation of the initial groundwater table, likely because a higher initial groundwater table leads to higher initial water content in the upper vadose zone, which facilitates more water to move toward the freezing front by shortening its flow path. It can also be noted that when ice content is higher, it releases a greater amount of latent heat, slowing down the freezing front propagation.

5.4. Effect of Solute Transport

Dissolved solutes (e.g., chloride, potassium, nitrate, etc.) in unfrozen water can affect soil freezing characteristics by changing the freezing point, which in turn affects the movement of water flow and solute transport. S0 is again considered a baseline scenario for comparison because it has a fairly low concentration throughout the entire simulation period indicating that heat transfer is hardly impacted by solute distribution and transport. Here three scenarios S4a∼S4c with higher initial and background solute concentrations (100 mol · m^{-3}) are designed to analyze the effect of solute transport properties on soil freeze-thaw processes. The other simulation conditions are again the same as those in Section 4. The variation of solute concentration in the sand soil layer is found to be unremarkable because of minimal water content and little water movement in the upper vadose zone such that its simulation results are not displayed.

Figure 13 shows the evolution of solute concentration in the clay and silt soil layers during the freeze-thaw cycles. It can be seen that the spreading of the averaged concentration front is clearly illustrated in the larger dispersivity scenario S4a in Figure 13a. The solutes are concentrated in the residual unfrozen pore water within the frozen zone, but their concentrations gradually decrease during the thawing stage yet maintain a relatively high value

near the zone of the maximum frost depth. This trend becomes much more significant in the silt than in the clay as the dispersivity increases (Figure 13b), and no adsorption occurs (Figure 13c). The concentrated solutes in the upper silt soil layer will migrate downward along with the infiltration of thawed-water during the thawing stage, which leads to low concentration close to the ground surface. In contrast, a relatively high concentration still appears close to the ground surface of the clay during the thawing stage. This is because the water flux in the clay during the thawing stage is minimal (Figures 7a and 8b), and the evaporation rate is relatively large (Figure 6b). It should be noted that the solute may continue to migrate upward along with the moisture if high evaporation occurs during the thawing stage, which can then accumulate in the upper soil layers potentially resulting in topsoil salinization. In terms of the groundwater dynamics, the intensity of groundwater level fluctuation becomes weaker because the freezing point is depressed by the higher solute concentrations, particularly for scenario S4c, involving the silt soil with a lower dispersivity and no adsorption. Simultaneously, the heat transfer was impacted by these slight changes in freezing point, which caused small variations in deformation, although there is no noticeable evolution trend. It should be noted that these slight but existing variations would become more significant if the solute concentration in soil water had been initially increased by potential mass sources such as fertilizer infiltration in agricultural soil or road salt in urban areas.

6. Model Assumptions, Limitations, and Future Considerations

As noted in the model formulation description and explanation of the simulation domain and boundary conditions, a series of assumptions were made to simplify the governing equations for water and vapor flow, heat transfer, and deformation in unsaturated freezing soil. Although these assumptions were considered physically reasonable, they will influence the numerical results. The shallow model domain employed for this analysis is commonly utilized and considered suitable for most soil profiles in seasonally frozen regions and within the upper zones of a permafrost active layer (e.g., Cui et al., 2020; Shoop & Bigl, 1997; Xie et al., 2021; Zheng et al., 2002). However, the actual depth of soil layers and local landscape features (topography/hillslope variations) could be accommodated to obtain a more realistic initialization and configuration for field-scale land surface-subsurface systems (e.g., Elshamy et al., 2020). Although the shallow simulation domain and short simulation duration permitted an examination of the interaction between the integrated, physics-rich, multi-processes of interest during freeze-thaw cycles for the purposes of the current study, the relevant model configurations would need to be adjusted (scaled-up) depending on the nature of the subsurface system and research objectives being considered.

The very fine grid discretization and short time steps utilized in these numerical experiments are computationally demanding. This fine level of discretization was utilized in order to explore the complex interactions between the various processes of interest associated with dynamic freeze-thaw cycles. Part of the goal of the current study was to more completely understand the interaction between the different inter-related processes and also to attempt to identify which precesses are crucial/necessary for accurate prediction of phenomena of interest at various scales. This would help inform improved parameterization of land surface and Earth system models applied at larger, more realistic scales in multiple dimensions.

In the current study, the simplifying assumptions are also adopted relative to the surface-subsurface boundary conditions, and a highly simplified flow system was utilized for the numerical experiments. For example, this study neglects possible subsurface lateral flow, surface runoff, and other mass sources/sinks (e.g., snow/rainfalls, groundwater pumping, and irrigation). For larger-scale and longer-term simulation scenarios, these processes will need to be included and will be part of a subsequent study. In addition, the intermittent infiltration through the fully- or partially-frozen ground surface when the snow melts in the early spring or during extreme weather events (in winter, late spring, or late fall in cold regions) should be examined in subsequent studies. Imbibition of heavy rainfall or ponded water may reduce the effective stress of the soil and influence shallow soil water storage, which can significantly affect the various coupled mass transport processes in the subsurface during subsequent freeze-thaw cycles.

The soil profiles examined in this study assumed homogeneity, and the impact of heterogeneous, layered soil profiles with various different textures would also be of interest in subsequent work to derive conclusions that are more general and comprehensive (e.g., Carsel & Parrish, 1988; Chung & Horton, 1987; Williams & Smith, 1989). Moreover, the selected soil characteristic curve is an empirical formula, and its shape is assumed to be invariant with other factors such as soil suction, and mechanical and chemical variations (reactive solutes). Furthermore, the hysteretic behavior of the freeze-thaw cycle, vegetation dynamics, and possible occurrences of ice lenses (wedges) and/or excess ice are also neglected. Finally, in the case when loading/unloading actions are

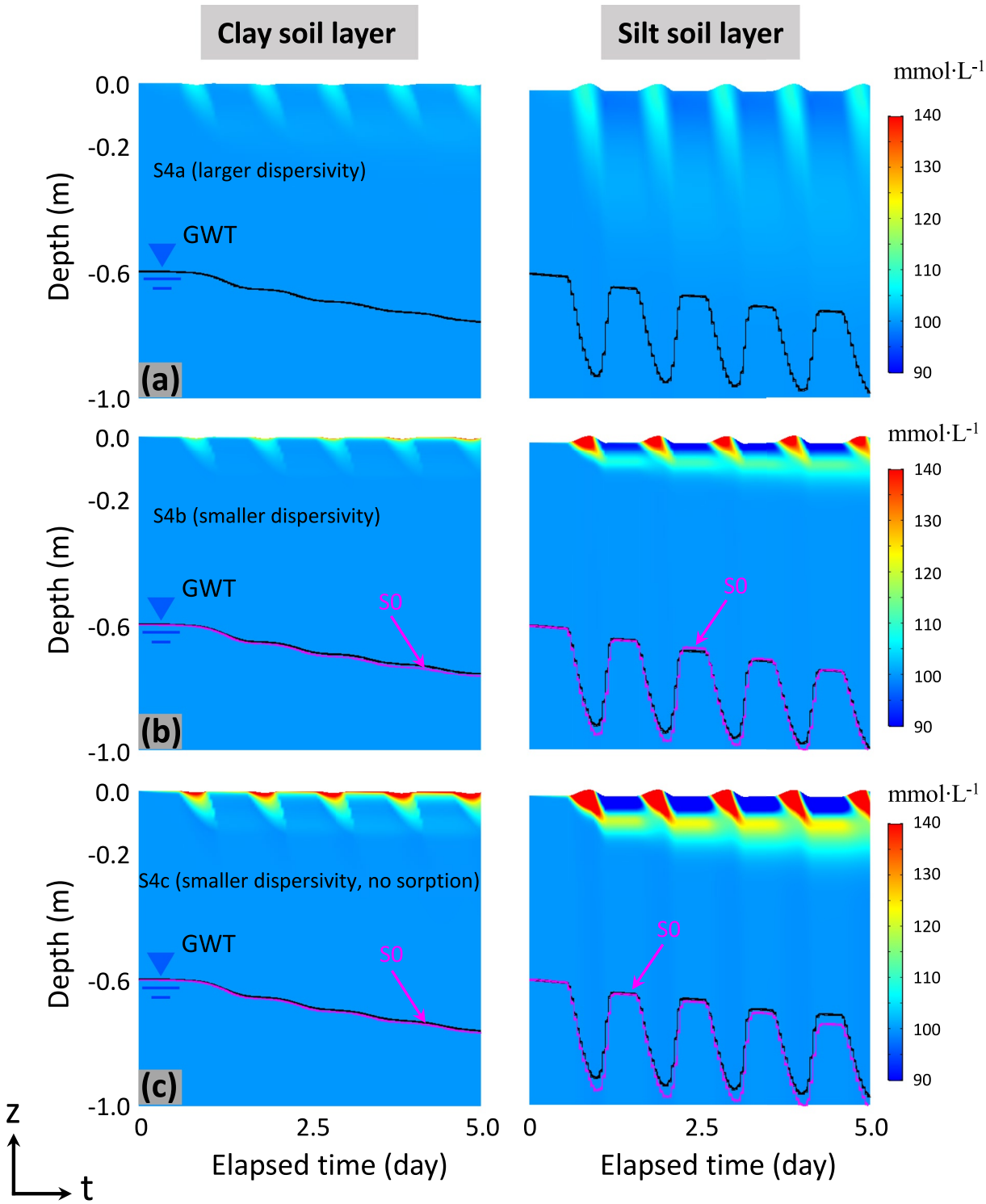

Figure 13. The effect of solute transport properties on the tracer concentration distribution in the clay and silt soil layers during the freeze-thaw cycles. From top to bottom, the panels show concentration contours of (a) larger dispersivity with adsorption (S4a), (b) smaller dispersivity with adsorption (S4b), and (c) smaller dispersivity without adsorption (S4c), respectively. The simulated groundwater table (magenta lines) for the baseline case S0 was also overlaid in (b) and (c) for comparison. The deformation was also projected on the contour plots with vertical displacements exaggerated by a factor of 5.

taking place on the ground surface, the modeling framework presented in this paper must be supplemented with an appropriate constitutive component that is able to simulate non-elastic deformations.

7. Summary and Implications

Efforts toward modeling of water (moisture)-vapor flow, thermal regime, solute migration, and deformation evolution in variably-saturated soil during freeze-thaw cycles have not, so far, yielded a constitutive model that would be accepted widely by subsurface hydrologists. The model framework presented in this work belongs to the category of coupled thermal-hydraulic-mechanical-chemical processes based on continuum mechanics assumptions, which is among the first to permit the development of a numerical model to examine the influence of soil freeze-thaw processes on the interaction between soil water and groundwater, frost heave and thaw settlement, and solute transport (and reactions) in the subsurface. The model capabilities were verified by comparing the simulation results to laboratory experimental observations from the published literature. The proposed THM-C model was utilized to simulate water and vapor flow, heat transfer, deformation, and solute transport during periodic freeze-thaw cycles in three distinct soil types under partially saturated conditions, and the effects of relevant factors on soil behavior were analyzed. Several main points were drawn from this work, as follows:

1. A bidirectional exchange occurs between groundwater in the saturated zone and soil water in the vadose zone during freeze-thaw cycles, which causes a similar fluctuating pattern of soil displacement and solute concentration. The fluctuations of groundwater levels are most significant in the silt owing to the greater cryosuction compared with the low permeable clay and the low water-holding capacity sand.
2. Vapor flow in the freezing sand is much more significant than that in the freezing silt or clay. The rapid dewatering ahead of the freezing front causes local volume shrinkage when the freezing front propagates downward during the freezing stage, and this volume shrinkage is gradually recovered when the thawed water replenishes the water loss zone during the thawing stage.
3. The transient profiles of soil moisture, temperature, displacement, and solute concentration during freeze-thaw cycles are sensitive to the changes in amplitude and freeze-thaw period of the sinusoidal varying air temperature near the ground surface, the hydraulic conductivity of soil textures, and the initial groundwater levels. The solute is concentrated in the residual pore water within the frozen zone (due to solute exclusion from the ice phase). Its concentration gradually decreases with the arrival of the thawing stage, yet it maintains a relatively high value near the area of maximum frost penetration depth (at the end of the freezing stage).

Cyclic freeze-thaw of water or other liquids in porous media is a ubiquitous phenomenon and affects areas as diverse as the cryo-relevant Earth (or Mars) sciences, physics, chemistry, biology and materials sciences, and engineering practices. In general, our results suggest that it is essential to consider the coupled thermal-hydraulic-mechanical-chemical behavior when computing water and energy dynamics in the cryo-subsurface, especially for those small scales. In agricultural areas with a shallow groundwater table depth, for example, crop productivity related to the availability of soil nutrients for crops grown outside of the summer season (e.g., winter wheat and other cover crops) can be affected by the water-vapor exchange between the vadose zone and groundwater during the freeze-thaw period. The coupled modeling approach presents a potential research strategy with which to target poorly understood aspects of soil nutrient cycling under a changing climate.

Data Availability Statement

Experimental data sets for this research were obtained from Loli et al. (2020), Wu (2017), and Wang et al. (2016).

Acknowledgments
The authors gratefully acknowledge funding from the Natural Sciences and Engineering Research Council of Canada (NSERC) through a Discovery Grant awarded to David Rudolph. We also acknowledge the financial support from the Global Water Futures program (GWF) through the Northern Water Futures project and the GWF Core Modeling. We are grateful for the technical advice and funding provided by the Government of the Northwest Territories Environmental Studies Research Fund. Constructive suggestions and comments from three anonymous reviewers, the Associate Editor and Editor Dr. Georgia Destouni considerably enhanced this article. We thank Los Alamos National Laboratory Research Library for providing open access funding support. This paper describes objective technical results and analysis. Any subjective views or opinions that might be expressed in the paper do not necessarily represent the views of the U.S. Department of Energy or the United States Government.

References

Arzanfudi, M. M., & Al-Khoury, R. (2018). Freeze–thaw of porous media: An extended finite element approach for soil freezing and thawing. *Advances in Water Resources*, *119*, 210–226. https://doi.org/10.1016/j.advwatres.2018.07.013

Bai, R., Lai, Y., Zhang, M., & Yu, F. (2018). Theory and application of a novel soil freezing characteristic curve. *Applied Thermal Engineering*, *129*, 1106–1114. https://doi.org/10.1016/j.applthermaleng.2017.10.121

Biermans, M. B. G. M., Dijkema, K. M., & De Vries, D. A. (1976). Water movement in porous media towards an ice front. *Nature*, *264*(5582), 166–167. https://doi.org/10.1038/264166a0

Boulet, G., Braud, I., & Vauclin, M. (1997). Study of the mechanisms of evaporation under arid conditions using a detailed model of the soil–atmosphere continuum. Application to the EFEDA I experiment. *Journal of Hydrology*, *193*(1–4), 114–141. https://doi.org/10.1016/s0022-1694(96)03148-4

Campbell, G. S. (1977). *An introduction to environmental biophysics*. Springer-Verlag.

Carsel, R. F., & Parrish, R. S. (1988). Developing joint probability distributions of soil water retention characteristics. *Water Resources Research*, *24*(5), 755–769. https://doi.org/10.1029/wr024i005p00755

Chen, J., Gao, X., Zheng, X., Miao, C., Zhang, Y., Du, Q., & Xu, Y. (2019). Simulation of soil freezing and thawing for different groundwater table depths. *Vadose Zone Journal*, *18*(1), 1–14. https://doi.org/10.2136/vzj2018.08.0157

Chin, L. Y., Raghavan, R., & Thomas, L. K. (2000). Fully coupled geomechanics and fluid-flow analysis of wells with stress-dependent permeability. *SPE Journal*, *5*(01), 32–45. https://doi.org/10.2118/58968-pa

Chung, S. O., & Horton, R. (1987). Soil heat and water flow with a partial surface mulch. *Water Resources Research*, *23*(12), 2175–2186. https://doi.org/10.1029/wr023i012p02175

Comsol. (2017). *User's guide*. Version 5.3. Comsol. Retrieved from http://www.comsol.com

Corapcioglu, M. Y., & Panday, S. (1995). Multiphase approach to thaw subsidence of unsaturated frozen soils: Equation development. *Journal of Engineering Mechanics*, *121*(3), 448–459. https://doi.org/10.1061/(asce)0733-9399(1995)121:3(448)

Coussy, O. (2005). Poromechanics of freezing materials. *Journal of the Mechanics and Physics of Solids*, *53*(8), 1689–1718. https://doi.org/10.1016/j.jmps.2005.04.001

Cui, L., Zhu, Y., Zhao, T., Ye, M., Yang, J., & Wu, J. (2020). Evaluation of upward flow of groundwater to freezing soils and rational per-freezing water table depth in agricultural areas. *Journal of Hydrology*, *585*, 124825. https://doi.org/10.1016/j.jhydrol.2020.124825

Dall'Amico, M., Endrizzi, S., Gruber, S., & Rigon, R. J. T. C. (2011). A robust and energy-conserving model of freezing variably-saturated soil. *The Cryosphere*, *5*(2), 469–484. https://doi.org/10.5194/tc-5-469-2011

De Vries, D. A. (1958). Simultaneous transfer of heat and moisture in porous media. *Eos, Transactions American Geophysical Union*, *39*(5), 909–916. https://doi.org/10.1029/tr039i005p00909

Elshamy, M. E., Princz, D., Sapriza-Azuri, G., Abdelhamed, M. S., Pietroniro, A., Wheater, H. S., & Razavi, S. (2020). On the configuration and initialization of a large-scale hydrological land surface model to represent permafrost. *Hydrology and Earth System Sciences*, *24*(1), 349–379. https://doi.org/10.5194/hess-24-349-2020

Evans, S. G., Ge, S., Voss, C. I., & Molotch, N. P. (2018). The role of frozen soil in groundwater discharge predictions for warming alpine watersheds. *Water Resources Research*, *54*(3), 1599–1615. https://doi.org/10.1002/2017wr022098

Frampton, A., & Destouni, G. (2015). Impact of degrading permafrost on subsurface solute transport pathways and travel times. *Water Resources Research*, *51*(9), 7680–7701. https://doi.org/10.1002/2014wr016689

Grenier, C., Anbergen, H., Bense, V., Chanzy, Q., Coon, E., Collier, N., et al. (2018). Groundwater flow and heat transport for systems undergoing freeze–thaw: Intercomparison of numerical simulators for 2D test cases. *Advances in Water Resources*, *114*, 196–218. https://doi.org/10.1016/j.advwatres.2018.02.001

Hansson, K., Šimůnek, J., Mizoguchi, M., Lundin, L. C., & van Genuchten, M. T. (2004). Water flow and heat transport in frozen soil: Numerical solution and freeze-thaw applications. *Vadose Zone Journal*, *3*(2), 693–704. https://doi.org/10.2136/vzj2004.0693

Hayashi, M. (2013). The cold vadose zone: Hydrological and ecological significance of frozen–soil processes. *Vadose Zone Journal*, *12*(4), vzj2013-03. https://doi.org/10.2136/vzj2013.03.0064

Hillel, D. (1971). *Soil and water: Physical principles and processes*. Academic Press.

Huang, X., Andrews, C. B., Liu, J., Yao, Y., Liu, C., Tyler, S. W., et al. (2016). Assimilation of temperature and hydraulic gradients for quantifying the spatial variability of streambed hydraulics. *Water Resources Research*, *52*(8), 6419–6439. https://doi.org/10.1002/2015wr018408

Huang, X., & Rudolph, D. L. (2021). Coupled model for water, vapour, heat, stress and strain fields in variably saturated freezing soils. *Advances in Water Resources*, *154*, 210–226. https://doi.org/10.1016/j.advwatres.2021.103945

Huang, X., & Rudolph, D. L. (2022). A hybrid analytical-numerical technique for solving soil temperature during the freezing process. *Advances in Water Resources*, *162*, 104163. https://doi.org/10.1016/j.advwatres.2022.104163

Huang, X., Rudolph, D. L., & Glass, B. (2022). A coupled thermal-hydraulic-mechanical approach to modeling the impact of roadbed frost loading on water main failure. *Water Resources Research*, *58*(3), e2021WR030933. https://doi.org/10.1029/2021wr030933

Ingebritsen, S. E., Sanford, W. E., & Neuzil, C. E. (2006). *Groundwater in geologic processes*. Cambridge University Press.

Ireson, A. M., van Der Kamp, G., Ferguson, G., Nachshon, U., & Wheater, H. S. (2013). Hydrogeological processes in seasonally frozen northern latitudes: Understanding, gaps and challenges. *Hydrogeology Journal*, *21*(1), 53–66. https://doi.org/10.1007/s10040-012-0916-5

Karra, S., Painter, S. L., & Lichtner, P. C. (2014). Three-phase numerical model for subsurface hydrology in permafrost-affected regions (PFLOTRAN-ICE v1. 0). *The Cryosphere*, *8*(5), 1935–1950. https://doi.org/10.5194/tc-8-1935-2014

Kelleners, T. J. (2020). Coupled water flow, heat transport, and solute transport in a seasonally frozen rangeland soil. *Soil Science Society of America Journal*, *84*(2), 399–413. https://doi.org/10.1002/saj2.20036

Kurylyk, B. L., MacQuarrie, K. T., & Voss, C. I. (2014). Climate change impacts on the temperature and magnitude of groundwater discharge from shallow, unconfined aquifers. *Water Resources Research*, *50*(4), 3253–3274. https://doi.org/10.1002/2013wr014588

Lein, W. A., Slone, S. M., Smith, C. J. E., Bernier, A. P., & Oren, J. I. (2019). *Frost depth penetration and frost heave in frost susceptible soils*. ERDC Cold Regions Research Laboratory.

Liu, Q., & Hu, R. (2017). Simulation of heat and mass transfer during artificial ground freezing in saturated saline groundwater. In *Proceedings of the 2017 COMSOL conference in Rotterdam*.

Loli, M., Tsatsis, A., Kourkoulis, R., & Anastasopoulos, I. (2020). A simplified numerical method to simulate the thawing of frozen soil [Dataset]. Proceedings of the Institution of Civil Engineers-GeoEngineering, *173*(5), 408–427. https://doi.org/10.1680/jgeen.18.00239

Lu, N., & Likos, W. J. (2004). *Unsaturated soil mechanics*. Wiley.

McKenzie, J. M., Voss, C. I., & Siegel, D. I. (2007). Groundwater flow with energy transport and water–ice phase change: Numerical simulations, benchmarks, and application to freezing in peat bogs. *Advances in Water Resources*, *30*(4), 966–983. https://doi.org/10.1016/j.advwatres.2006.08.008

Merlin, O., Stefan, V. G., Amazirh, A., Chanzy, A., Ceschia, E., Er-Raki, S., et al. (2016). Modeling soil evaporation efficiency in a range of soil and atmospheric conditions using a meta–analysis approach. *Water Resources Research*, *52*(5), 3663–3684. https://doi.org/10.1002/2015wr018233

Michalowski, R. L. (1993). A constitutive model of saturated soils for frost heave simulations. *Cold Regions Science and Technology*, *22*(1), 47–63. https://doi.org/10.1016/0165-232x(93)90045-a

Mohammed, A. A., Bense, V. F., Kurylyk, B. L., Jamieson, R. C., Johnston, L. H., & Jackson, A. J. (2021). Modeling reactive solute transport in permafrost–affected groundwater systems. *Water Resources Research*, *57*(7), e2020WR028771. https://doi.org/10.1029/2020wr028771

Moldrup, P., Olesen, T., Gamst, J., Schjønning, P., Yamaguchi, T., & Rolston, D. E. (2000). Predicting the gas diffusion coefficient in repacked soil water–induced linear reduction model. *Soil Science Society of America Journal*, *64*(5), 1588–1594. https://doi.org/10.2136/sssaj2000.6451588x

Molson, J. W., & Frind, E. O. (2015). *HEATFLOW-SMOKER: Density-dependent flow and advective-dispersive transport of thermal energy, mass or residence time* (p. 116). Univ. Laval and Univ. Waterloo.

Mualem, Y. (1976). A new model for predicting the hydraulic conductivity of unsaturated porous media. *Water Resources Research*, *12*(3), 513–522. https://doi.org/10.1029/wr012i003p00513

Noborio, K., McInnes, K. J., & Heilman, J. L. (1996). Two–dimensional model for water, heat, and solute transport in furrow–irrigated soil: II. Field evaluation. *Soil Science Society of America Journal*, *60*(4), 1010–1021. https://doi.org/10.2136/sssaj1996.03615995006000040008x

Oke, T. R. (2002). *Boundary layer climates*. Routledge.

Philip, J. R., & De Vries, D. A. (1957). Moisture movement in porous materials under temperature gradients. *Eos, Transactions American Geophysical Union*, *38*(2), 222–232. https://doi.org/10.1029/tr038i002p00222

Selvadurai, A. P., & Suvorov, A. P. (2017). *Thermo-poroelasticity and geomechanics*. Cambridge University Press.

Serne, R. J. (2007). *Kd values for agricultural and surface soils for use in Hanford site farm, residential, and river shoreline scenarios*. Pacific Northwest National Laboratory.

Shoop, S. A., & Bigl, S. R. (1997). Moisture migration during freeze and thaw of unsaturated soils: Modeling and large scale experiments. *Cold Regions Science and Technology*, *25*(1), 33–45. https://doi.org/10.1016/s0165-232x(96)00015-8

Šimůnek, J., Šejna, M., Saito, H., Sakai, M., & van Genuchten, M. T. (2018). *The HYDRUS-1D software package for simulating the movement of water, heat, and multiple solutes in variably saturated media*. Version 4.17. HYDRUS Software Series 3 (p. 315). Dept. of Env. Sci., Univ. of Calif. Riverside.

Thomas, H. R., Cleall, P., Li, Y. C., Harris, C., & Kern-Luetschg, M. (2009). Modelling of cryogenic processes in permafrost and seasonally frozen soils. *Géotechnique*, *59*(3), 173–184. https://doi.org/10.1680/geot.2009.59.3.173

Tiedje, E. W., & Guo, P. (2011). Dewatering induced by frost heave in a closed system. In *Proceedings of the 15th international specialty conference on cold regions engineering, Quebec City, Que* (pp. 686–696). Canada. American Society of Civil Engineers.

Tubini, N., Gruber, S., & Rigon, R. (2021). A method for solving heat transfer with phase change in ice or soil that allows for large time steps while guaranteeing energy conservation. *The Cryosphere*, *15*(6), 2541–2568. https://doi.org/10.5194/tc-15-2541-2021

van de Griend, A. A., & Owe, M. (1994). Bare soil surface resistance to evaporation by vapor diffusion under semiarid conditions. *Water Resources Research*, *30*(2), 181–188. https://doi.org/10.1029/93wr02747

van Genuchten, M. T. (1980). A closed–form equation for predicting the hydraulic conductivity of unsaturated soils 1. *Soil Science Society of America Journal*, *44*(5), 892–898. https://doi.org/10.2136/sssaj1980.03615995004400050002x

Wang, W., Wang, L., Yu, F., & Wang, Q. (2016). One dimensional thaw consolidation behaviors with periodical thermal boundaries [Dataset]. KSCE Journal of Civil Engineering, *20*(4), 1250–1258. https://doi.org/10.1007/s12205-015-0419-8

Williams, P. J., & Smith, M. W. (1989). *The frozen Earth: Fundamentals of geocryology*. Cambridge University Press.

Winterfeld, P. H., & Wu, Y. S. (2020). An overview of our coupled thermal-hydrological-mechanical simulator for porous and fractured media. In *54th U.S. rock mechanics/geomechanics symposium*. OnePetro.

Wu, H. (2017). Experimental study of nitrate transport characteristics during the freeze-thaw process in the vadose zone. M.Sc. thesis [Dataset]. Zenodo. China University of Geosciences, Beijing (In Chinese with English abstract). https://doi.org/10.5281/zenodo.8145489

Xie, H. Y., Jiang, X. W., Tan, S. C., Wan, L., Wang, X. S., Liang, S. H., & Zeng, Y. (2021). Interaction of soil water and groundwater during the freezing-thawing cycle: Field observations and numerical modeling. *Hydrology and Earth System Sciences*, *25*(8), 4243–4257. https://doi.org/10.5194/hess-25-4243-2021

Yu, F., Guo, P., Lai, Y., & Stolle, D. (2020). Frost heave and thaw consolidation modelling. Part 2: One-dimensional thermohydromechanical (THM) framework. *Canadian Geotechnical Journal*, *57*(10), 1595–1610. https://doi.org/10.1139/cgj-2019-0306

Žák, A., Beneš, M., & Illangasekare, T. H. (2013). Analysis of model of soil freezing and thawing. *International Journal of Applied Mathematics*, *43*(3), 127–134.

Zhang, S., Teng, J., He, Z., Liu, Y., Liang, S., Yao, Y., & Sheng, D. (2016). Canopy effect caused by vapour transfer in covered freezing soils. *Géotechnique*, *66*(11), 927–940. https://doi.org/10.1680/jgeot.16.p.016

Zheng, X., Fan, G., & Xing, S. (2002). *Water movement in seasonal unsaturated freeze–Thaw soil*. Geological Publishing House. (In Chinese).